Physical Mechanisms of Ocean Variability in Key Regions

Peter Brandt

Kumulative Habilitationsschrift
vorgelegt bei der Mathematisch-Naturwissenschaftlichen Fakultät
der Christian-Albrechts-Universität zu Kiel

Kiel, 2004

Contents

1 Introduction

In this paper physical mechanisms of ocean variability in key regions of the thermohaline and wind-driven circulation will be discussed that are thought to be important for a better understanding of ocean circulation dynamics. The present study is aimed at understanding a wide range of physical processes of ocean variability including mesoscale eddies, gravity and planetary ocean waves. These different processes are analyzed using a variety of different methods such as in-situ hydrographic and current observations, satellite remote sensing and numerical modeling. On the one hand observational results are needed for critical testing of ocean models, while, on the other hand, there is an increasing importance of ocean models as key instruments for the physical understanding of ocean variability that can hardly be comprehensible on the basis of observations alone (Böning and Semtner 2001). A large part of the data used in the present paper were collected during the World Ocean Circulation Experiment (WOCE), including the satellite altimeter missions. WOCE was aimed at understanding the World Ocean circulation and its relation to climate on a global basis. As a main result, however, the WOCE data have shown the extremely active time-dependence of the ocean circulation (Wunsch 2001). The role of the highly variable ocean dynamics, and in particular of the oceanic mesoscale, for the mean circulation and stratification is largely unknown. Recently, several studies that are based on theoretical and laboratory work focused on the role of the mesoscale eddy field in setting the stratification of the World Ocean (Marshall et al. 2002). The importance of eddy-induced diapycnal fluxes could be shown for the transport and stratification of the Circumpolar Current (Karsten et al. 2002) or for the maintenance of the thermocline (Radko and Marshall 2004). The main focus of the present study is the understanding of aspects of the observed large ocean variability, its role in the mean circulation as well as its long-term changes. The paper consists of three parts: the first part deals with the annual cycle and planetary wave propagation, the second part with the instability of the mean current system and the mesoscale eddy field, and the third part with shorter period ocean variability due to oceanic tides and strait dynamics.

A large part of the ocean variability is generated by the action of the wind at the sea surface. As a direct mechanism, wind stress curl variability on time scales from months to years leads to the generation of planetary Rossby waves resulting in a change of the mean meridional transport in the ocean interior and thus establishing a changed basin wide Sverdrup circulation (Willebrand et al. 1980). At the equator, variations in the zonal wind speed lead to the generation of equatorial Kelvin and Rossby waves and concurrently to a redistribution of heat and mass along the equator (Philander 1978). In the first part of this study we discuss in-situ as well as remote observations of annual off-equatorial Rossby waves in the Arabian Sea. These Rossby waves are radiated from the western side of the Indian subcontinent, but are continuously forced by the wind stress curl over the central Arabian Sea. While the strength of the mean deep meridional overturning in the northern Indian Ocean is still under debate (Schott and McCreary 2001), the presence of the observed Rossby waves suggests a strong time-dependence of the meridional overturning at least in the central Arabian Sea due to a seasonal redistribution of the deep water masses. In a second case of directly wind-driven ocean variability, we study the annual cycle in the equatorial Atlantic Ocean using repeated ship sections, remote sensing data as well as results of a regional numerical model. In this case we focus on the downward propagation of equatorial Rossby and Kelvin waves along descending equatorial beams generating distinct maxima of variability at depth. These beams that are reproduced in numerical models (McCreary 1984; Thierry et al. 2003) may explain the large seasonal variability observed in the depth range of the Equatorial Intermediate Current (EIC, Boebel et al. 1999; Schott et al. 2003). The simulated year-to-year changes in the amplitude of the annual cycle can be traced back to a part of the interannual

variability of the wind field that is mainly associated with the Pacific El Nino phenomenon. The individual research papers that are the basis of the first part of the submitted paper are:

Brandt, P., L. Stramma, F. Schott, J. Fischer, M. Dengler, and D. Quadfasel, Annual Rossby waves in the Arabian Sea from TOPEX/Poseidon altimeter and in-situ data, *Deep-Sea Res. II,* **49,** 1197-1210, 2002a.

Brandt, P., and C. Eden, Annual cycle and interannual variability of the mid-depth tropical Atlantic Ocean, accepted in *Deep-Sea Res. II*, 2004.

A more indirect mechanism by which the wind generates ocean variability on time scales from days to months and length scale from several kilometers to several hundred kilometers results from the barotropic or baroclinic instability of the wind-driven currents (Stammer and Wunsch 1999). While there also exists directly wind-generated eddy energy that is of particular importance in regions of low energy levels, the instability mechanism along frontal zones is the main source of eddy kinetic energy (EKE) in the World Ocean (Stammer et al. 2001). The seasonal to interannual variability in the strength of the eddy fields indicates on the one hand a variability in the strength of the generating currents, on the other hand it may also induce a variability in the hydrographic fields due to the associated varying horizontal mixing between contributing water masses. Stammer et al. (2004) concluded that changes of eddy intensity as observed by altimetry must be of concern in long climate simulations. In the second part of the present study we analyze moored hydrographic and current observations as well as remotely sensed sea surface height data from the Somali basin and the Arabian Sea. This region, being one of the most energetic regions of the World Ocean, is characterized by the presence of the Great Whirl during the Southwest Monsoon (Fischer et al. 1996). Schott and McCreary (2001) pointed out in their review paper that most of the details concerning the generation, persistence and decay or collapse of this eddy are still poorly understood. Here the analysis of the different in-situ and remote sensing data sets is presented that revealed the presence of strong deep-reaching, intraseasonal fluctuations in the region of the Great Whirl. While the seasonal cycle of the strength of the intraseasonal fluctuations in that region can be explained by the seasonal variations in the (locally and remotely) wind-driven current system, the strong year-to-year variability of the intraseasonal fluctuations is mainly generated by the intrinsic ocean dynamics and cannot be simply explained by variations in the atmospheric forcing (Wirth et al. 2002). Another study that is based on sea surface height data from altimetry regards the eddy field in the subpolar North Atlantic. In the central Labrador Sea a large part of the eddy kinetic energy is imported from the West Greenland Current region (Lilly et al. 2003), where it is probably generated by the barotropic instability of the boundary current as suggested by high-resolution numerical simulations (Eden and Böning 2002). The observed seasonal to interannual variability is studied here with respect to the seasonal variations in the strength of the subpolar gyre and interannual variations of aspects of the thermohaline circulation like, e.g., the deep convection in the central Labrador Sea. The individual research papers that are the basis of the second part of the submitted paper are:

Brandt, P., M. Dengler, A. Rubino, D. Quadfasel, and F. Schott, Intraseasonal variability in the southwestern Arabian Sea and its relation to the seasonal circulation, *Deep-Sea Res. II,* **50,** 2129 – 2141, 2003.

Brandt, P., F. Schott, A. Funk, and C. S. Martins, Seasonal to interannual variability of the eddy field in the Labrador Sea from satellite altimetry, *J. Geophys. Res.*, **109**, C02028, doi:10.1029/2002JC001551, 2004b.

The third part of the present study regards the tidally induced dynamics and in particular the generation and propagation of internal solitary waves. These waves are generated by the interaction of the barotropic tides with topographic features like sills or bathymetric

slopes. Due to the advent of satellite remote sensing it became evident that tidally generated solitary waves are ubiquitous along continental margins, around islands, in sea straits and estuaries (Apel et al. 1995). Besides their local importance for the mixing of different water masses, they might also constitute a dissipation mechanism for global tides (Munk and Wunsch 1998). Here, we analyze velocity data obtained in the tropical Atlantic Ocean showing large-amplitude internal solitary waves superimposed on the North Equatorial Counter Current (NECC). In sea straits or estuaries that are characterized by an hydraulically controlled exchange flow the generation of internal solitary waves is in general associated with the periodic flooding of the control. Moreover, the tidal dynamics influence the strength of the mean exchange flow (Farmer and Armi 1986; Helfrich 1995). To understand long-term changes in the Mediterranean sea level (Ross et al. 2000), we analyzed output fields of a numerical tidal model of the Strait of Gibraltar that is able to simulate the tidal dynamics and the mean exchange flow. This model was used to explain observed trends in the mean sea level of the western Mediterranean as the result of long-term changes in the density difference between Atlantic inflow and Mediterranean outflow. The individual research papers that are the basis of the third part of the submitted paper are:

Brandt, P., A. Rubino, and J. Fischer, Large-amplitude internal solitary waves in the North Equatorial Counter Current, *J. Phys. Oceanogr.*, **32,** 1567-1573, 2002b.

Brandt, P., A. Rubino, D. V. Sein, B. Baschek, A. Izquierdo, and J. O. Backhaus, Sea level variations in the western Mediterranean studied by a numerical tidal model of the Strait of Gibraltar, *J. Phys. Oceanogr.*, **34,** 433-443, 2004a.

2 Annual Cycle and Planetary Waves

2.1 Annual Rossby waves in the Arabian Sea

The Arabian Sea is characterized by a seasonal reversal of the wind field. During winter the winds of the Northeast Monsoon are directed away from the Asian continent, while during summer as part of the Southwest Monsoon there is a narrow atmospheric jet, the Findlater Jet that blows along the coast of Somalia and Oman. The seasonal cycle of the oceanic monsoon circulation in the Arabian Sea is characterized by vigorous changes of the Somali Current at its western margin (e.g., Schott and McCreary 2001), while in the interior of the Arabian Sea the monsoon related circulation variability is generally small. In winter, the Somali Current flows southward off Somalia, crossing the equator and is supplied by inflow through the passage between Socotra and the African continent in the north as well as out of the Arabian Sea from the east (Schott and Fischer 2000). In summer, the most prominent circulation feature is a large anticyclonic eddy, the *Great Whirl* (GW), which develops seasonally in the 5° to 10°N latitude range off northern Somalia after the onset of the summer monsoon and may last well into the transition period and even continue underneath the developing surface circulation of the winter monsoon. While the GW is mainly forced by local winds or by the wind stress curl over the interior Arabian Sea (Schott 1983), remote effects propagating in from the west cost of India appear to be relevant (McCreary et al. 1993, Bruce et al. 1994; Shankar and Shetye 1997). Bruce et al. (1994) described the elevation of the sea surface in January near India as the Laccadive High (LH), an anticyclonic gyre that develops off the southwest coast of India just north of the Laccadives. They found a westward translation of the LH by January with a subsequent dissipation in midbasin. During the summer monsoon, the LH is replaced by a region of low sea level, the Laccadive Low (LL).

The meridional overturning circulation in the northern Arabian Sea is characterized by a large annual cycle. While in the annual mean the northern Arabian Sea is a net heat exporter, in winter there is a net heat import into the northern hemisphere (Garternicht and Schott 1997). The mechanism through which this seasonal reversal of the meridional heat transport occurs is to a large degree attributed to the seasonal reversal of the meridional Ekman transports but vertical shear consisting largely of thermal wind shear balanced by zonal density gradients and small ageostrophic shear also appears to contribute (Lee and Marotzke 1998; Schott and McCreary 2001). Stramma et al. (2002) analyzed two hydrographic sections taken during summer monsoon of August 1993 (Sonne cruise 89, SO89) and during the winter monsoon of January 1998 (Sonne cruise 128, SO128) along approximately 8°N.

In the upper 300 to 450 m a seasonally reversing shallow meridional overturning cell appeared to exist in which the Ekman transport (Fig. 2.1) is balanced by a geostrophic transport. The heat flux across 8°N is dominated by the Ekman transport, yielding about -0.6 PW for August 1993, and 0.24 PW for January 1998. These values are comparable to climatological and model derived heat flux estimates (Garternicht and Schott 1997). At larger depth a vertical overturning cell of about 4 to 6 Sv was determined for both cruises with inflow below 2500 m and outflow between about 300 m and 2000 m. These estimates of the deep meridional overturning require large deep upwelling velocities that, at the moment, cannot by explained by available estimates of deep diapycnal mixing in that region (see, e.g., Schott and McCreary 2001).

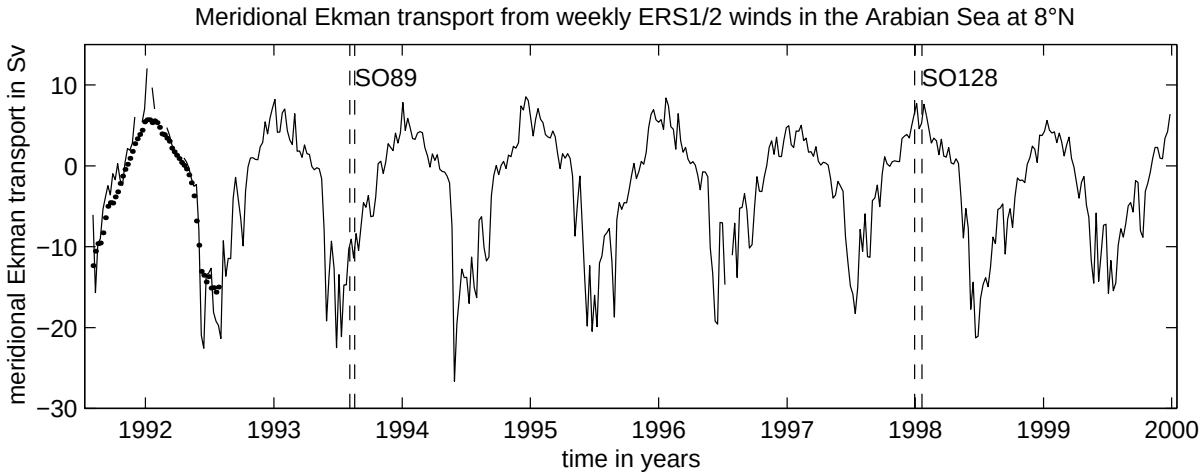

Fig. 2.1. Time series of meridional Ekman transport across 8°N in the Arabian Sea between 50.5°E and 79.5°E from the ERS scatterometer weekly wind fields (solid). The mean seasonal cycle of the meridional Ekman transport derived from all measurements is shown for the first year (dots). The time periods of the two cruises SO89 in August 1993 and SO128 in January 1998 are marked by dashed lines (from Stramma et al. 2002).

Recently, Beal et al. (2003) estimated a much smaller deep overturning circulation of about 1 Sv based on two sections along 8.5°N in the Arabian Sea. They applied an inverse model with the constriction that the deep upwelling velocities adjust within $\pm 5 \times 10^{-5}$ cm/s. These different estimates suggest that there are still large uncertainties resulting from the use of different sections or the choice of the wind field for the estimate of the Ekman transport, but also from the treatment of the data, like e.g. the choice of the geostrophic reference, the treatment of the diapycnal fluxes in inverse studies, or the treatment of the bottom triangles.

A strong seasonality of the sea surface height (SSH) is associated with the seasonal cycle in the wind field of the northern Indian Ocean (Fig. 2.2). The annual harmonic in the Arabian Sea can be delineated as a band of enhanced amplitude in the latitude range 6° to 10°N with its maximum elevation in January near India and in June near Africa. In this area the annual harmonic is the dominant signal in the SSH and explains more than 60 percent of the total variance. This band of enhanced amplitude was interpreted by Subrahmanyam et al. (2001) as first and second baroclinic mode Rossby waves propagating westward from the western side of the Indian subcontinent towards Africa. McCreary et al. (1993) concluded from different numerical simulations of the Indian Ocean that a large part of the seasonal variability in the Arabian Sea, in particular the Rossby wave in the eastern Arabian Sea propagating away from the west coast of India, is primarily remotely forced by the winds in the Bay of Bengal. However, there is also a local maximum in the band of enhanced amplitude of the annual harmonic of the SSH in the Arabian Sea at about 60°E (see Fig. 2.2a). While this local maximum cannot be explained by the radiation of free Rossby waves from the eastern boundary as these waves must gradually decay during their propagation (Qiu et al. 1997), it can rather be explained by local Rossby wave generation due to the seasonal varying wind curl field. The annual signal in the wind stress curl is dominant only in the southwestern part of the Arabian Sea. There, the maximum negative wind stress curl is found in July, caused by the strong winds of the Southwest Monsoon. The annual Rossby waves in the Arabian Sea should thus not be seen as free Rossby waves simply radiating from the western side of the Indian subcontinent, but as Rossby waves that are continuously forced by the wind stress curl over the central Arabian Sea.

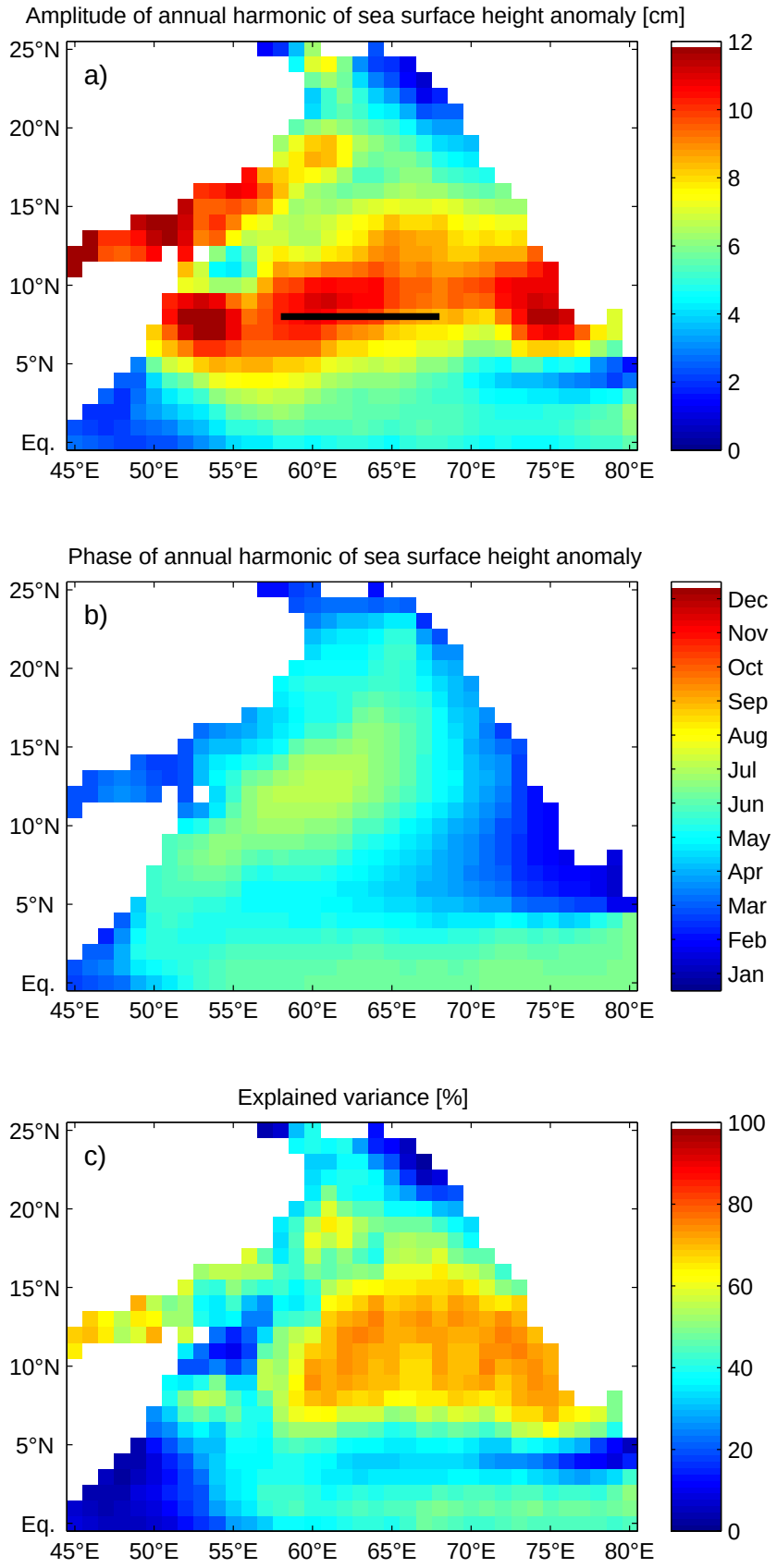

Fig. 2.2. Amplitude of the annual cycle of the TOPEX/Poseidon SSH (a), month of its maximum elevation (b), and percentage of total variance contained in the annual cycle (c). The black line in (a) gives the location of the density sections analyzed in the following. The hydrographic data were acquired from two cruises by RV Sonne in August 1993 and in January 1998 (from Brandt et al. 2002a).

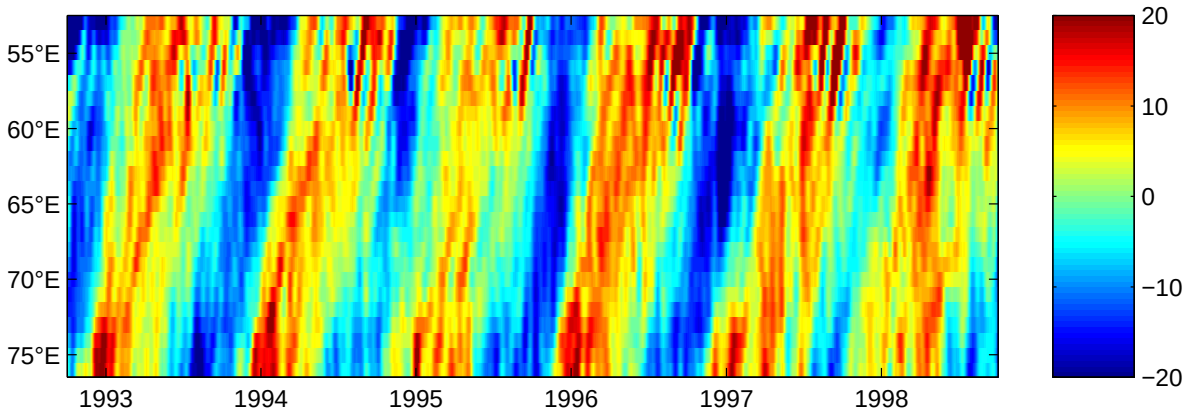

Fig. 2.3. Longitude-time plot of TOPEX/Poseidon SSH anomaly [cm] at 8°N (from Brandt et al. 2002a).

The longitude-time plot of the SSH anomaly at 8°N mainly reflects the annual cycle of westward propagating SSH elevations and depressions generated near India during each year (Fig. 2.3). However, there are considerable smaller-scale signals of monthly to bimonthly periods that propagate westward superimposed on the annual signal. They are visible off the west coast of India, are weak in the interior of the Arabian Sea, and are strongly amplified near the African coast. The strong fluctuations near the African coast are connected to the evolution of the GW generated with the onset of the Southwest Monsoon in May and will be further discussed in section 3.1. In this section we want to focus on the annual signal that can also be found in the hydrographic sections along 8°N that were analyzed by Stramma et al. (2002). In the following we will analyze only section data from the central part of the Arabian Sea. This restriction was necessary to avoid that strong circulation features like the GW on the western side of the Arabian Sea or the LH/LL on the eastern side of the Arabian Sea disturb our analysis with respect to annual Rossby waves. The chosen section extends from 58° to 68°E at 8°N in the central Arabian Sea.

The observed density difference for August 1993 compared to January 1998 shows significant larger-scale vertical and horizontal changes of the density anomaly (Fig. 2.4). In the upper 50 m of the water column a positive density anomaly can be observed, which results from the presence of different water masses in the near-surface layer during the different seasons: While in August the near-surface layer is occupied by salinity-rich Arabian Sea Water, in January salinity-poor water from the Bay of Bengal is transported into the Arabian Sea by the Northeast Monsoon Current. However, there are two striking features visible in the field of density difference that cannot be explained by seasonal variations in the water mass properties: 1) a negative density anomaly in the depth range 50 to 1000 m shallower in the eastern part and 2) a positive density anomaly underneath.

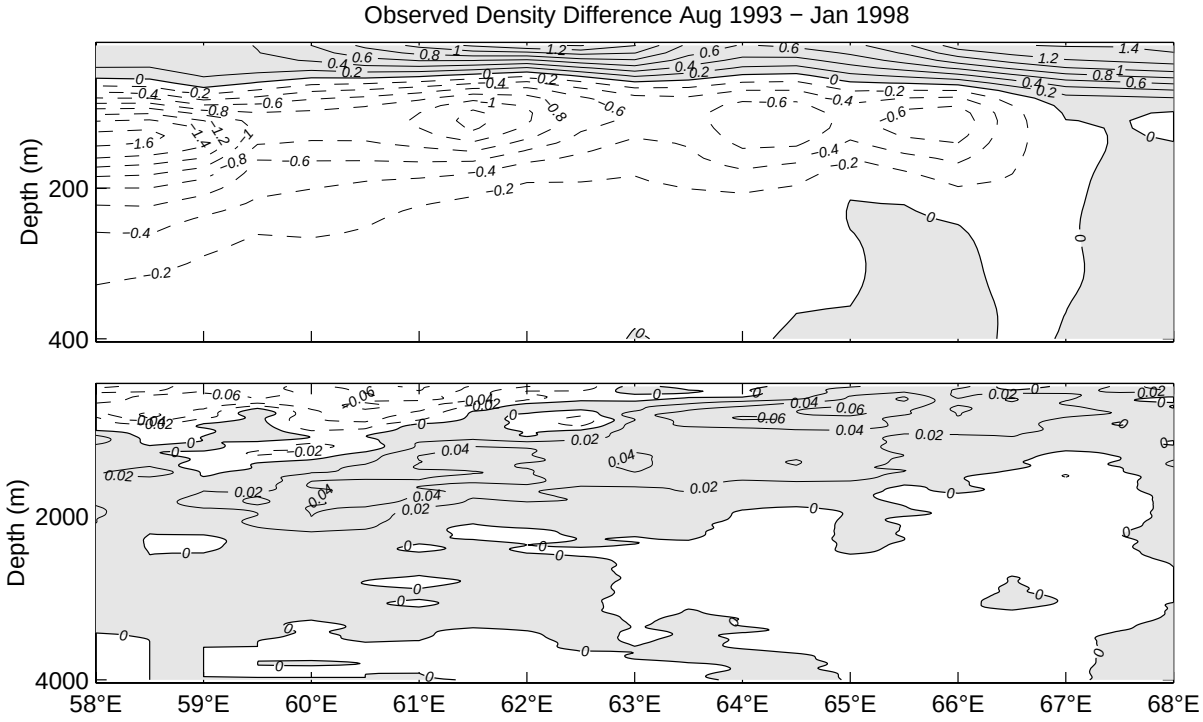

Fig. 2.4. Observed difference in density [kg/m³] for August 1993 compared to January 1998 (positive differences represent higher values in August 1993) for the central part of the 8°N section across the Arabian Sea. In the upper panel the density difference in the upper 400 m are shown, in the lower panel the density difference from 400 to 4000 m water depth with different contour intervals. The plotted data are vertically low pass filtered; the low pass wave number is 0.01 m^{-1} (from Brandt et al. 2002a).

The observed density fields were separated into contributions from different baroclinic modes. This mode decomposition is carried out by projecting each individual measured density profile onto density perturbation modes that are obtained from a mean Brunt-Väisälä-frequency profile. The amplitudes of the two lowest baroclinic modes are fitted between 58°E and 68°E by free Rossby wave solutions. These waves that result for an annual frequency and the observed corresponding baroclinic Rossby radius of deformation have wavelengths of 12 $\times 10^3$ and 4.4×10^3 km as well as phase velocities of 0.38 and 0.14 m/s, respectively. By using only first and second baroclinic mode Rossby waves the density fields are reconstructed. While the observed positive near-surface density anomaly cannot be explained by annual Rossby waves as expected, the signals in the observed density difference below the near-surface layer are well represented by signals in the reconstructed density difference. Looking at the whole water column, the reconstructed field of density difference explains 58% of total variance. When excluding the upper 100 m of the water column it explains even 87 % of total variance.

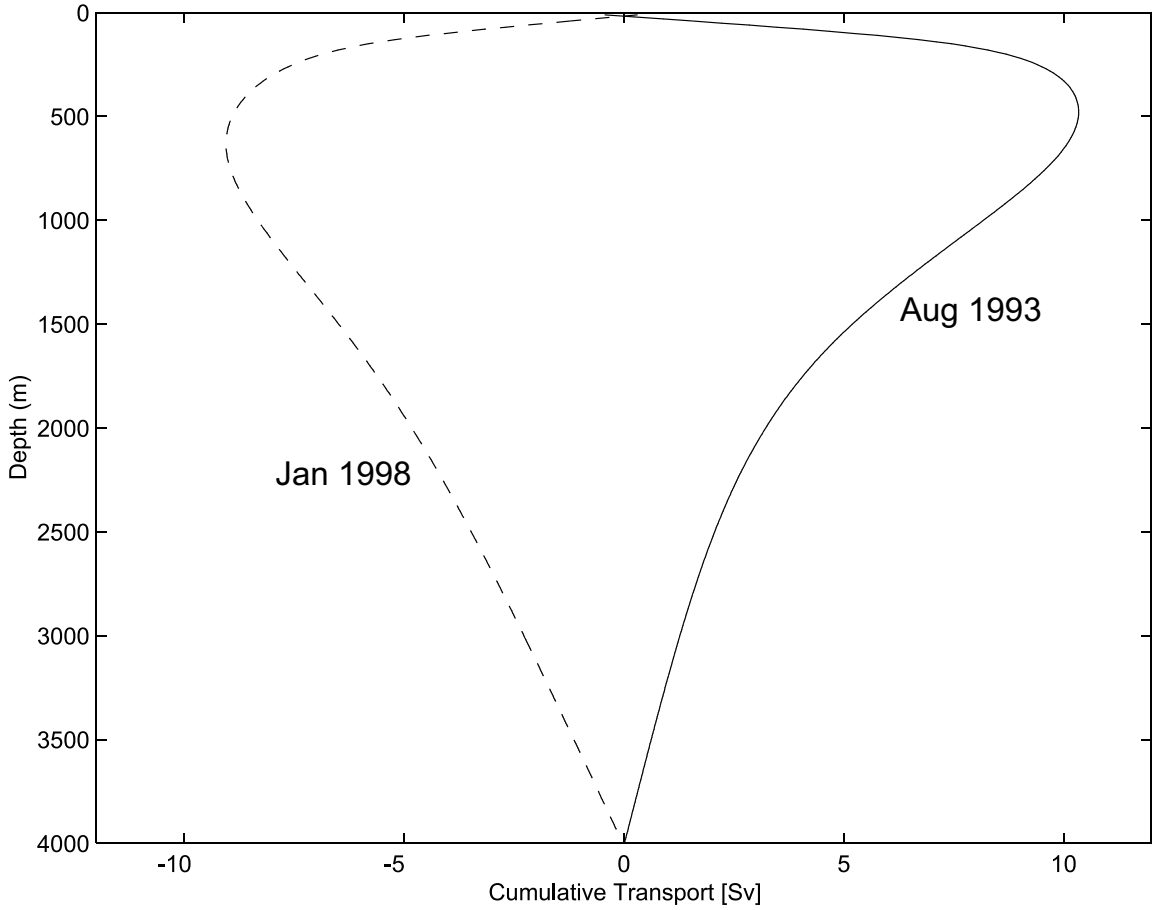

Fig. 2.5. Cumulative meridional transports along 8°N as integrated between 58° and 68°E and from the bottom to the sea surface for August 1993 (solid line) and January 1998 (dashed line) (from Brandt et al. 2002a).

The fitted Rossby wave solutions describe to a high degree the observed density fields that determine the geostrophic velocity fields. In fact, the propagation of the obtained first and second baroclinic mode annual Rossby waves results in seasonally reversing baroclinic transports that slosh water northward and southward (Fig. 2.5). The transport due to the annual Rossby waves at 8°N between 58° and 68°E in the upper 500 m of the water column is about 10 Sv to the south in August 1993 and about 10 Sv to the north in January 1998. Below 2000 m, there was still a northward transport of 3.2 Sv in August 1993 and a southward transport of 4.8 Sv in January 1998. Thus the annual Rossby waves generate the appearance of time-dependent meridional overturning cells that are superimposed on preexisting stationary meridional overturning cells (see, e.g., Lee and Marotzke 1998; Schott and McCreary 2001, Stramma et al. 2002).

2.2 Annual cycle in the Equatorial Atlantic

The equatorial Atlantic Ocean shows a significant seasonal cycle, essentially generated by the variable wind field. This pronounced seasonality is believed to play an important role in orchestrating tropical air-sea exchange and interaction as well as in the interhemispheric oceanic exchange of for example mass and heat. Moreover, the equatorial waveguide, establishing the family of equatorial waves, apparently favors the importance of a dynamical oceanic response to atmospheric forcing, such that the understanding of the mechanism and dynamics of the seasonal cycle and its long-term variability appears mandatory and interesting.

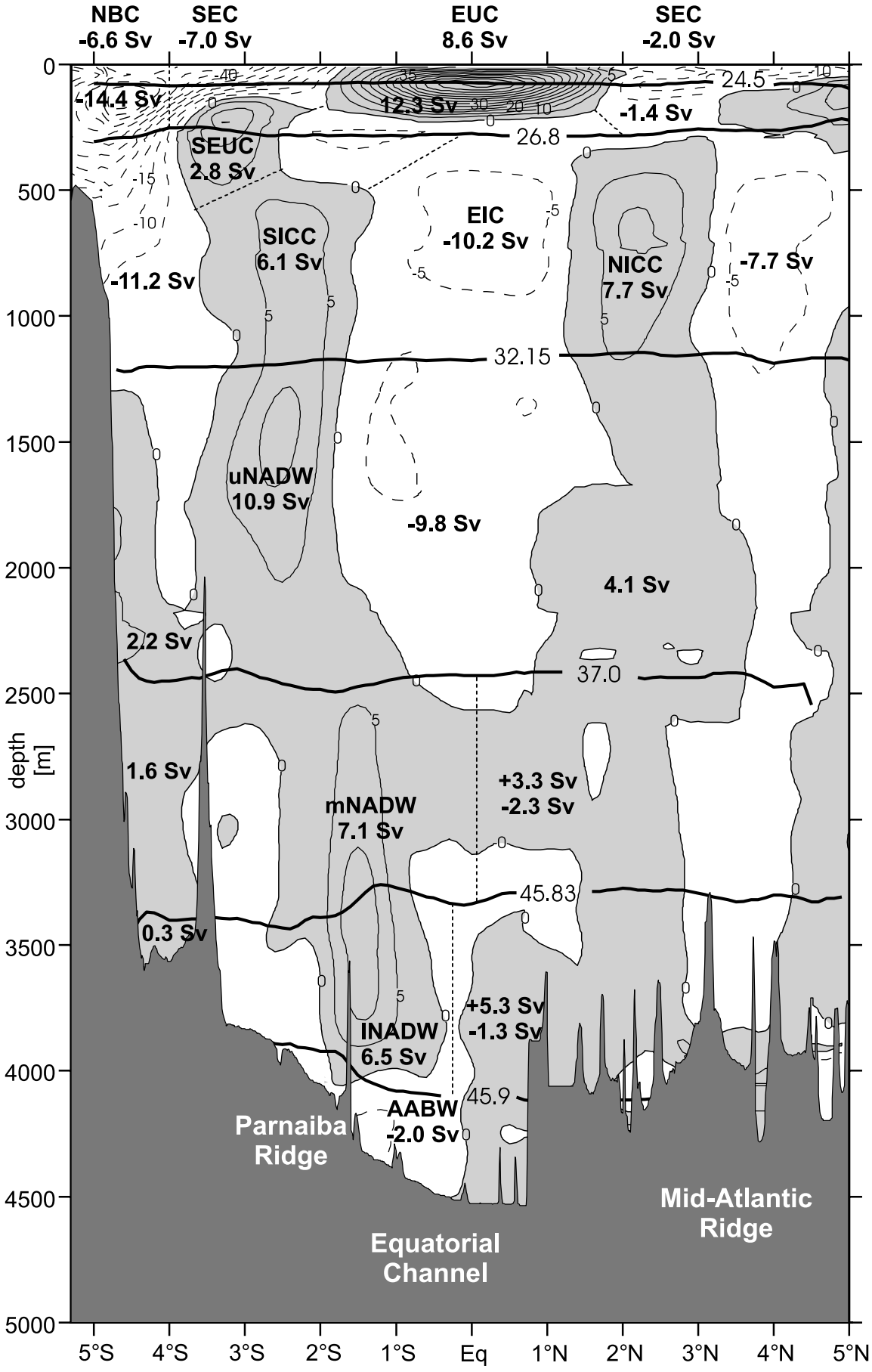

Fig. 2.6. Mean zonal current distribution across 35°W from 13 sections, with transports (in Sv = $10^6 m^3/s$) of the different current branches marked (from Schott et al. 2003).

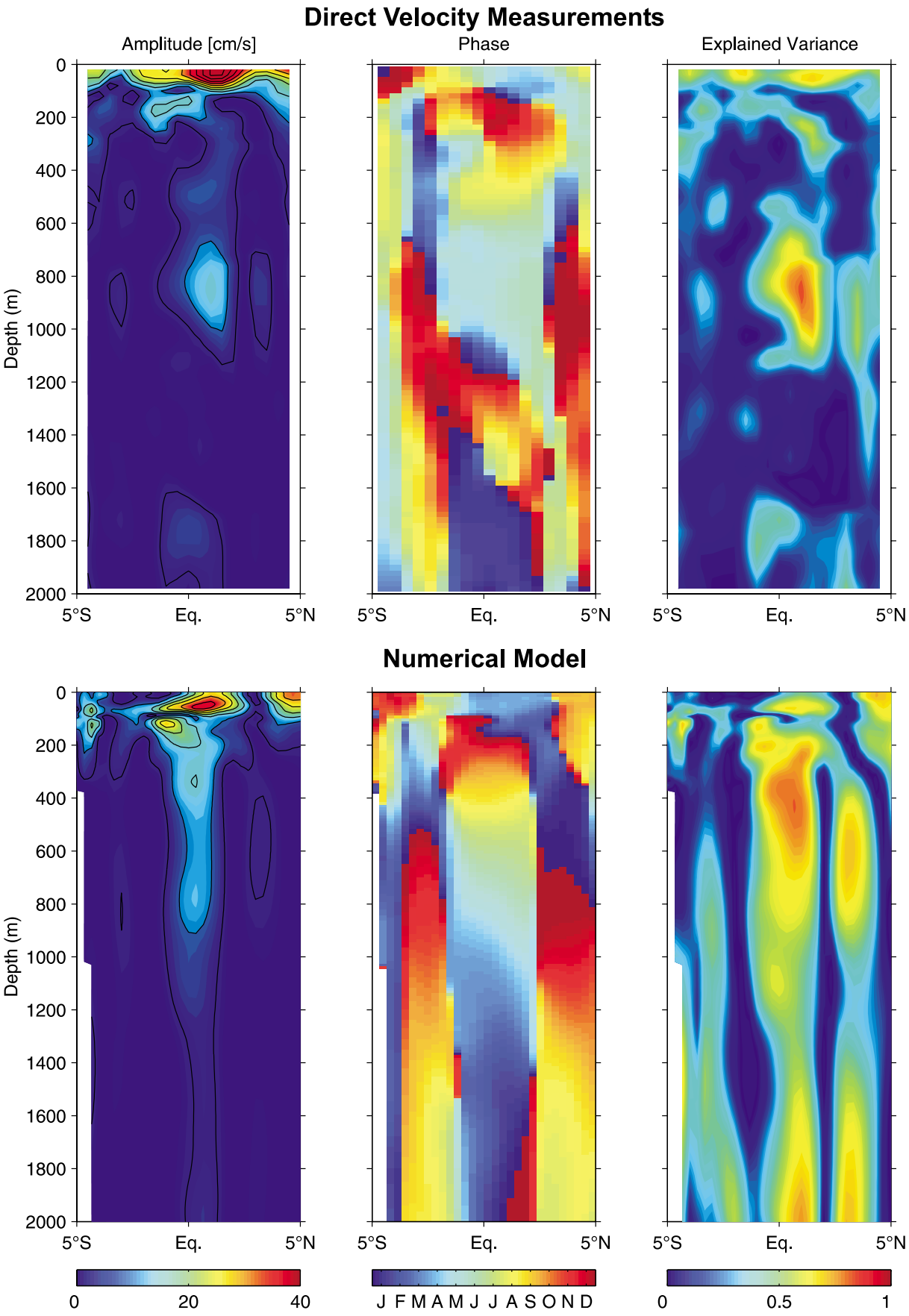

Fig. 2.7. Amplitude, phase and explained variance of the annual harmonic of the zonal velocity at 35°W as calculated from ship sections (upper panels) and as simulated by the numerical model (lower panels) (from Brandt and Eden 2004).

For the study of the annual cycle in the tropical Atlantic we use 13 cross-equatorial shipboard current profiling and hydrographic sections taken during the WOCE period between 1990 and 2002 along 35°W. The same sections are used in Schott et al. (2003) to determine the mean meridional structure of the zonal top-to-bottom circulation between the Brazilian coast, near 5°S, and 5°N and to estimate mean transports of the individual identified shallow, intermediate and deep current branches (Fig. 2.6). These transport calculations demonstrated that the 35°W section is a crucial bottle neck for the Atlantic overturning circulation with a net warm and intermediate water transport of 23 Sv to the east and a net NADW transport of 22 Sv to the west. The obtained numbers are of the same magnitude as quoted for the "conveyor belt" overturning circulation in the equatorial zone (Ganachaud and Wunsch 2000; Lux et al. 2001).

Figure 2.7 shows amplitude, phase and explained variance of the annual harmonic of the zonal velocity at 35°W derived from the same cross-equatorial shipboard sections (upper panels) and from a regional numerical model of the tropical Atlantic Ocean (lower panels). Below the near-surface layer, maxima of the annual harmonic amplitude of the observed zonal velocity at 35°W are found at the equator in about 500m, 900m, and 1800m depth. The phases at these depths are almost 6 months out of phase between the equator and 3-4° off the equator in both hemispheres. The maximum at 900m of about 15 cm/s, which is slightly shifted northward with respect to the equator, is part of the large seasonal variability of the zonal velocity in the depth range of the EIC between 400m and 1000m (see, e.g., Boebel et al. 1999; Schott et al. 2003). Within this depth range the phase of the annual harmonic shows an upward phase propagation with maximum eastward velocity at 900m depth in May and at 500m in August.

The annual harmonic of the simulated velocity field is calculated from monthly mean values of the 12 years model integration from 1990-2001. The amplitude of the annual harmonic of the simulated zonal velocity below 400m shows maximum values near the equator and secondary maxima at about 3-4° in both hemispheres (Fig. 2.7). In these two regions large values of the explained variance are found. The simulated maximum at the equator is shifted slightly northward, while the phase is symmetric and approximately 6 months out of phase at the equator with the region 3-4° in both hemispheres, i.e. the model results are in good agreement with the observations. The meridional structure of the annual harmonic of the zonal velocity, together with the upward phase propagation, indicate that the variability below the near-surface layer is dominated by downward propagating lowest odd meridional mode Rossby waves.

In order to show the space-time evolution of the annual cycle of the zonal velocity in the model and its interannual variations, it is convenient to use Principle Oscillation Patterns (POPs hereafter). The lower panels of Fig. 2.8 show the imaginary (sine) and real (cosine) spatial patterns of the POP (oscillation), while the upper panel shows the corresponding imaginary (sine) and real (cosine) time dependent coefficients of the POP. It is clear that the POP coefficients pick up the annual cycle of the zonal velocity. Note that this POP explains 70.7% of the total variance of the zonal velocity at this section. Interpreting the imaginary and real patterns and coefficients, we clearly see upward propagating velocity anomalies. Relating these velocity anomalies with a vertically and zonally propagating lowest odd meridional mode Rossby wave as before, the upward phase propagation means downward energy propagation, leading to the downward bend to the west of the velocity anomalies. The zonal wavelength of the downward propagating Rossby waves at intermediate depths might be estimated as twice the distance (at constant depth) between two zero crossings in the zonal velocity, i.e. about 9000 km. This wavelength yields a zonal phase velocity of roughly 0.3 m/s or about 6 months for a wave crest to cross the equatorial Atlantic basin. The

vertical structure of the zonal velocity, in particular the number of zero crossings of the POP in Fig. 2.8, indicates the dominance of the third and higher baroclinic modes.

The amplitude of the POP resembles the structure of "equatorial beams" described by McCreary (1984). The (square root of the) sum of both POP patterns (not shown) resembles the amplitude of the oscillation, comparable to the amplitude of the annual harmonic. The dominant structure in the amplitude of the POP is given by a shallow, east- and downward "Kelvin beam" and a deeper, west- and downward "Rossby beam", very similar to the linear theory in McCreary (1984) and the annual harmonic fit to the model results of Thierry et al. (2003). The Kelvin beam is thought to be directly wind-generated, bending eastward and downward, hitting the eastern boundary in about 50-100m depth. By reflection of the Kelvin wave activity, Rossby waves are generated at the eastern boundary forming the Rossby beam, which bends westward and downward. There is also a shallow, directly wind-generated Rossby beam present, propagating in the near surface layer westward and downward. The annual cycle of the zonal velocity at 35°W above 200m can be mainly explained by the directly wind-generated Rossby beam, while the deeper maxima in the depth range of the EIC is associated with the Rossby beam generated by the reflection of the Kelvin beam at the eastern boundary.

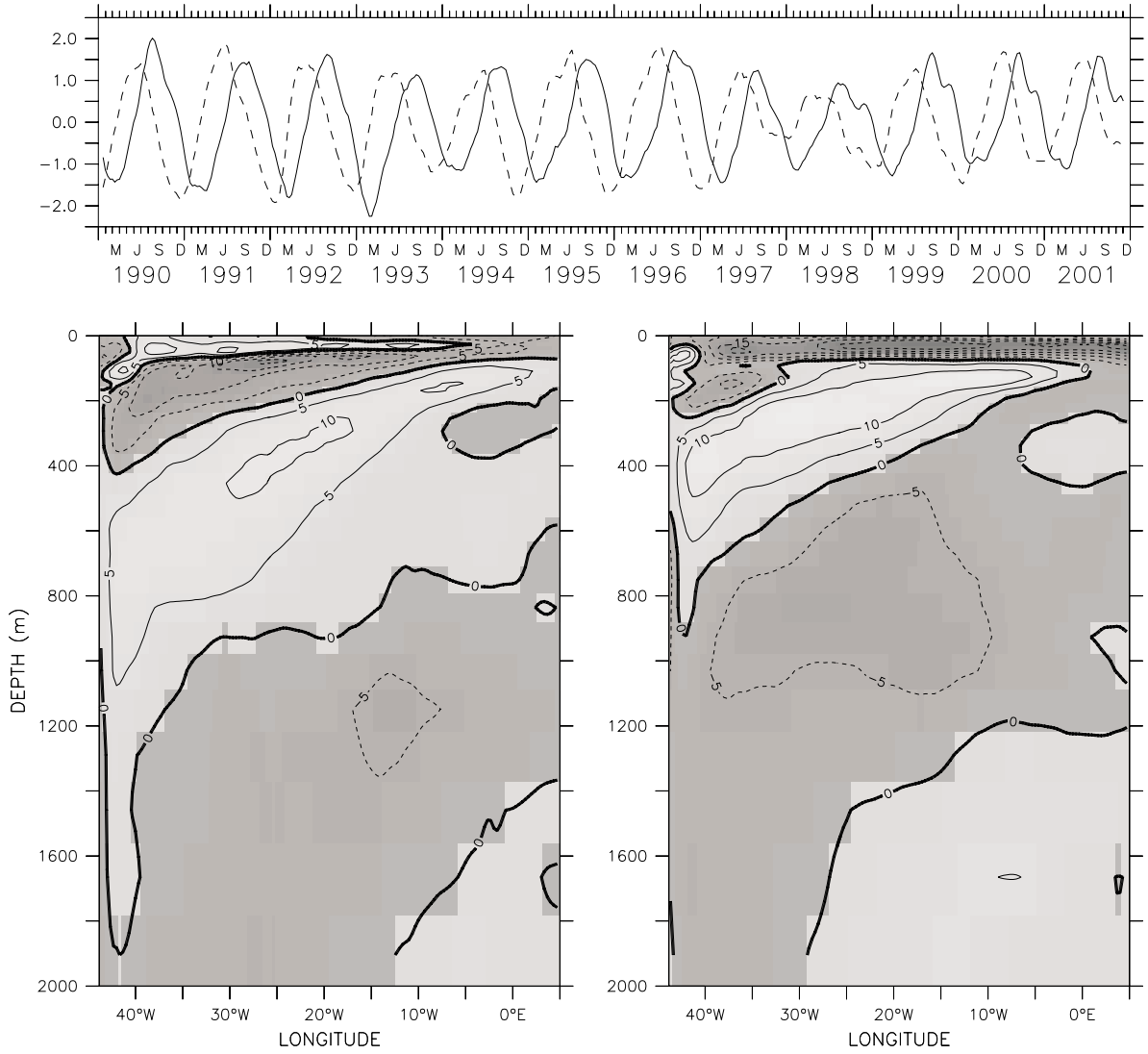

Fig. 2.8. Dominant POP of the simulated zonal velocity along the equator. Upper panel: The nondimensional POP coefficient (real part is given by the solid, imaginary part by the dashed line). Lower left panel: The imaginary part of the POP-pattern in cm/s. Lower right panel: The real part of the POP-pattern in cm/s. Contour interval is 5 cm/s (from Brandt and Eden 2004).

The analysis of the annual harmonic of the SSH as obtained from TOPEX/Poseidon altimetry indicate an east-west seesaw pattern similar to those obtained by linear models (Cane and Sarachik 1981; Weisberg and Tang 1990). Maximum correlation between the SSH gradient along the equator and the zonal wind speed at the equator is obtained at a lag of about 30 days (Fig. 2.9). The SSH gradient adjusts to variations in the zonal wind field due to the generation of lowest baroclinic modes equatorial waves having phase velocities that are consistent with those estimated from SSH data by França et al. (2003) to be 1.7 m/s for Kelvin waves and 0.6 m/s for Rossby waves.

On interannual time scales, the easterly winds are intensified in the western tropical Atlantic in response to Pacific warm events (Zebiak 1993; Latif and Barnett 1995). Associated with the strong Pacific El Nino, at the beginning of 1997 the south-easterly wind increases in the equatorial Atlantic (Vauclair and du Penhoat 2001) and led almost instantaneously to a decrease of the SSH gradient along the equator, i.e. elevated (depressed) SSH in the western (eastern) equatorial Atlantic. This reaction of the ocean to the varying wind forcing is associated with an almost instantaneous cease of the annual cycle of the SSH gradient (Fig. 2.9). In contrast, the POP coefficients of the zonal velocity field along the equator show a reduction of the annual cycle beginning in the second half of 1997 (Fig. 2.8). The obtained lag between the zonal wind anomaly at the equator and the variation of the amplitude of the annual cycle of the zonal velocity demonstrate the slower response of the velocity field at intermediate layers that is found to be dominated by higher baroclinic modes than the SSH field.

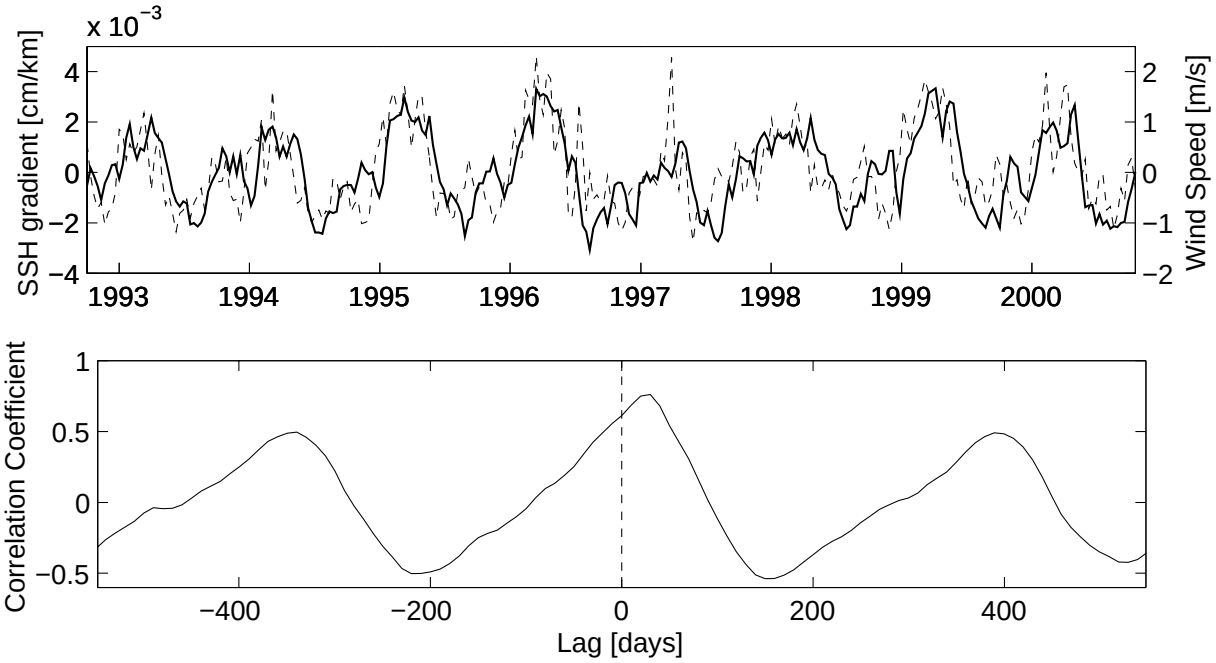

Fig. 2.9. Zonal wind speed along the equator averaged between 43°W and 8°E as observed by ERS scatterometer (dashed line, right axes, upper panel) and zonal gradient of TOPEX/Poseidon SSH calculated by an linear fit to SSH anomaly between 43°W and 8°E (solid line, left axes, upper panel). Time series sampled on a 10-day time grid are shown. In the lower panel a lag correlation between the two curves from the upper panel is shown; positive lag indicates SSH gradient lagging the zonal wind (from Brandt and Eden 2004).

3 Intraseasonal Variability and Mesoscale Eddy Field

3.1 Intraseasonal variability in the Arabian Sea

The Southern Gyre and the Great Whirl (GW) develop as large anticyclonic eddies in the southwestern Arabian Sea every year in response to the onset of the Southwest Monsoon (Swallow and Fieux 1982). They are part of the Somali Current system, one of the most energetic regions of the World Ocean, where surface currents of more than 3 m/s have been observed (Swallow and Bruce 1966; Schott 1983; Fischer et al. 1996). Both eddies, but in particular the GW, contribute substantially to the upwelling along the northern Somali coast and to the eastward transport of cold water into the interior Arabian Sea. As such, the GW is part of the upward branch of the shallow tropical-subtropical circulation cell in the Indian Ocean and strongly affects the heat balance of the Arabian Sea (Schott et al. 2002).

The GW itself is limited to the upper 1000 m of the water column. Most of the details concerning the generation, the persistence, and the decay or collapse of this eddy are still poorly understood (Schott and McCreary 2001). Rapid changes such as a sudden northward propagation of the Southern Gyre and coalescence with the GW have been observed during several years (Evans and Brown 1981), but in other years this two-gyre system remained in place and slowly decayed at the end of the Southwest Monsoon season. Until now this short-term and interannual variability could not be related in any simple way to variability in observed forcing fields, nor were numerical models able to realistically simulate the observed complex flow field in the area (Wirth et al. 2002). It appears, however, that intraseasonal variability plays a major role in the development of the seasonal cycle of the Somali Current.

In this investigation we present an analysis of TOPEX/Poseidon altimeter data and current and temperature data showing intraseasonal fluctuations in the GW region. The latter were collected during WOCE in 1995 and 1996 at the mooring array ICM-7 in the central Somali Basin. The dominant signal in the altimetric SSH data of the Arabian Sea is the annual cycle that was already discussed in section 2.1. The annual signal, which was interpreted as westward propagating, first and second baroclinic mode Rossby waves, can clearly be seen in the longitude-time plot of the SSH anomaly along 8°N (Fig. 2.3). However, near the coast of Somalia, smaller-scale signals of monthly to bimonthly periods were superimposed on the annual signal. Figure 3.1 shows the average SSH wavelet energy spectrum in a region close to the coast of Somalia between 52°E and 60°E and 5°N and 11°N. Overall, there was considerable year-to-year variability in the fluctuation strength of the wavelet energy as well as in its distribution among the different periods. In late summer and fall of each year, strong signals were found at periods between 30 and 50 days; significant signals at larger periods were only present during some years. The spatial distribution of the SSH wavelet energy at the period range between 38 and 45 days, corresponding to the central period range of the observed shorter-period fluctuations, is depicted in Fig. 3.2 for the different seasons of a mean annual cycle. High energy was found during summer and fall, while during winter and spring energy was relatively weak. Because significant SSH wavelet energy signals at this period range are found only in the northern Somali basin, which holds for periods ranging from 30 to 120 days, we suggest a local generation mechanism for the observed waves. A comparison with the theoretical cut-off period of Rossby waves shows that significant fluctuation energy was also present at the lower period range, where free baroclinic, linear Rossby waves cannot exist.

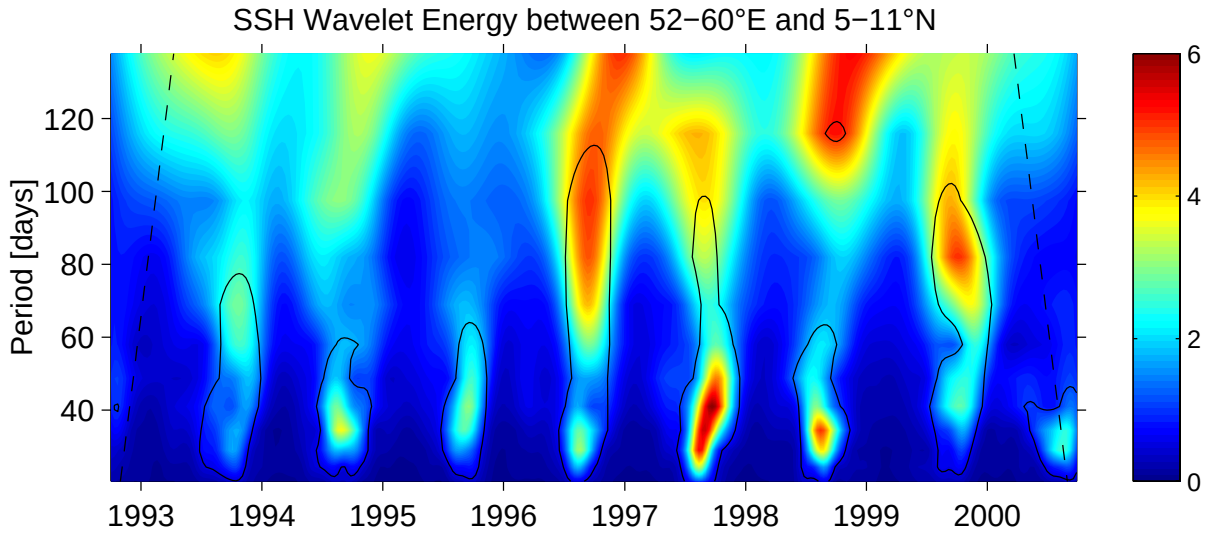

Fig. 3.1. Period-time plot of normalized SSH wavelet energy averaged between 52-60°E and 5-11°N. Solid lines marks the 95% significance level (from Brandt et al. 2003).

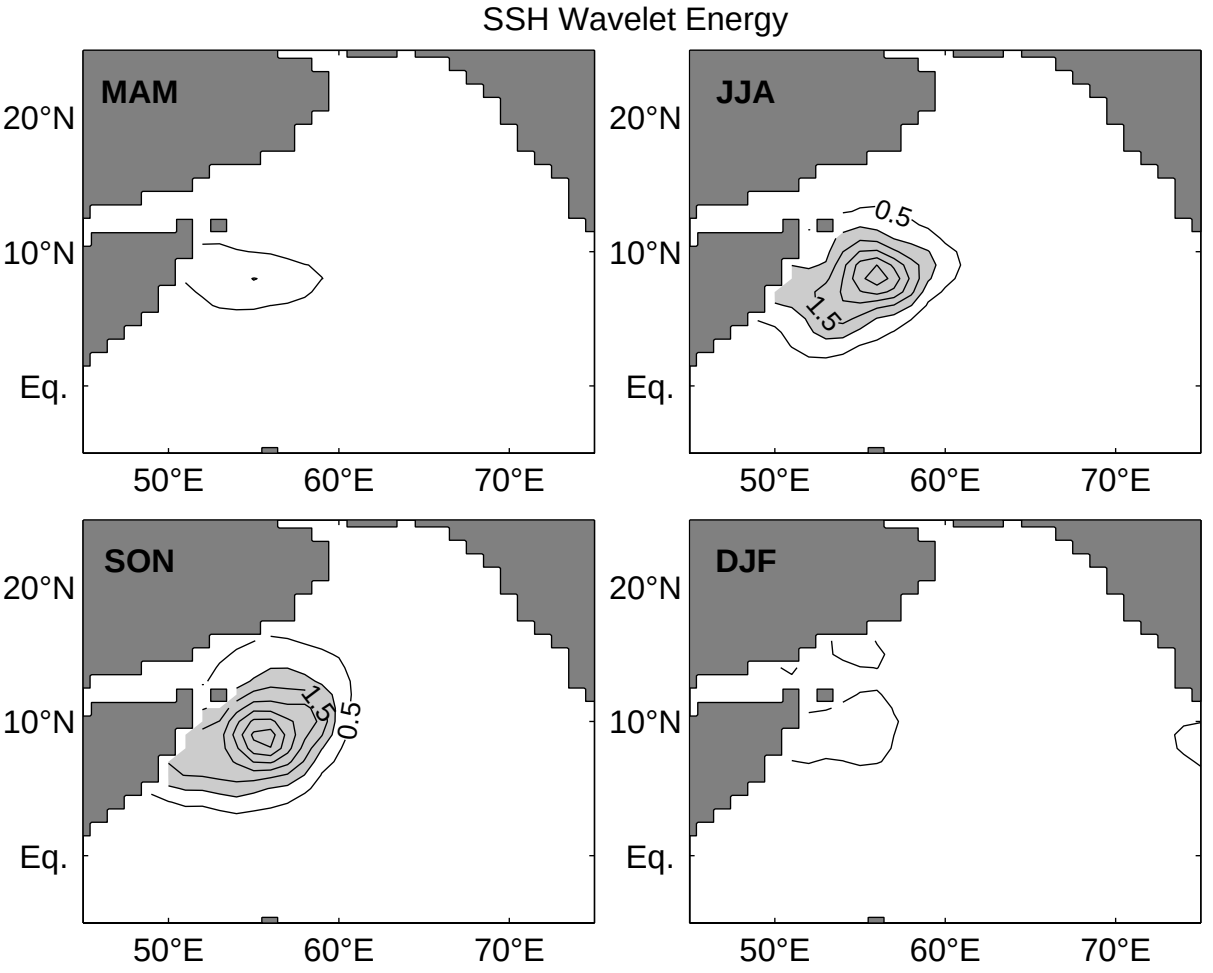

Fig. 3.2. Mean seasonal variation of the normalized SSH wavelet energy at the period range 38-45 days. The light gray shaded areas mark the regions with a significance level higher than 95% (from Brandt et al. 2003).

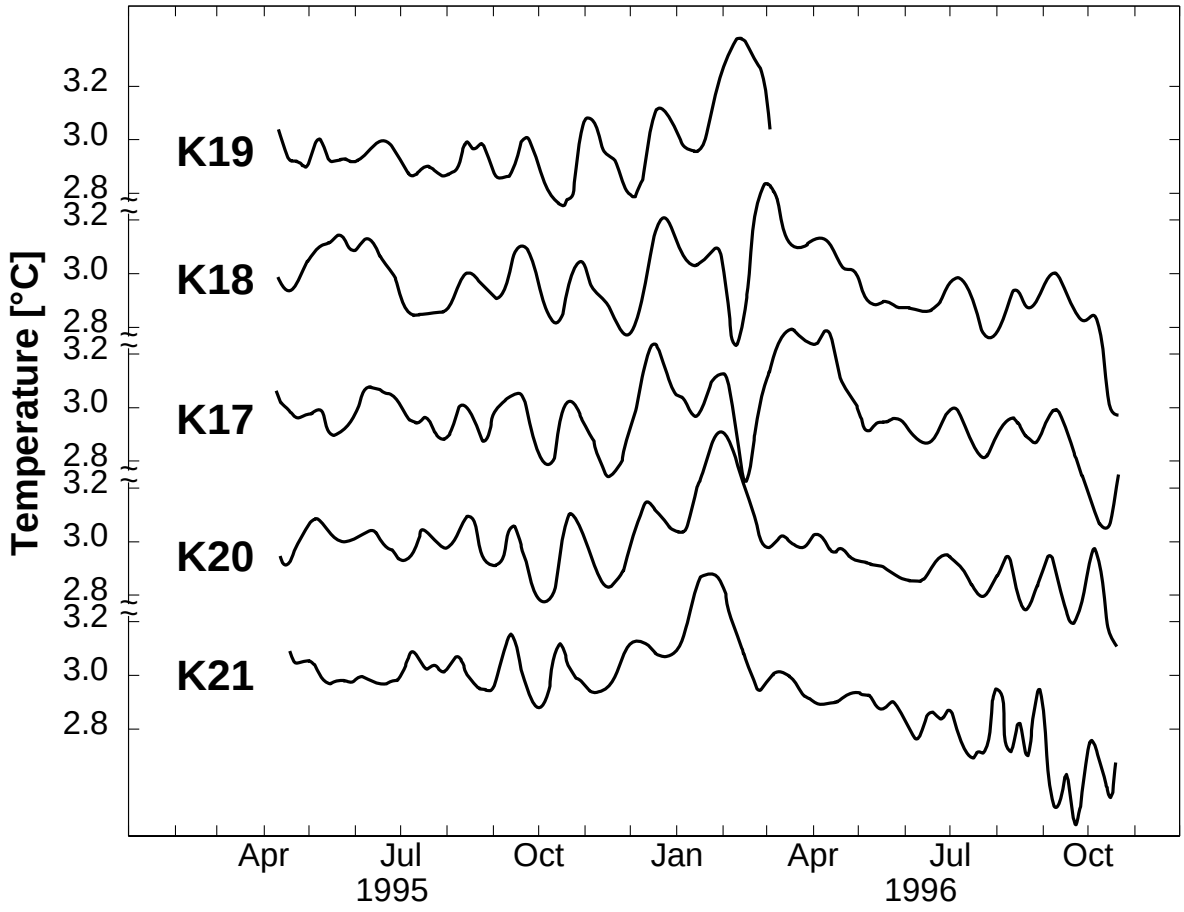

Fig. 3.3. Time series of temperature at 2000 m water depth at the five moorings K17 - K21 (from Brandt et al. 2003).

The in-situ data used in this study were collected in the southwestern Arabian Sea from April 1995 to October 1996 by moorings carrying Aanderaa rotor current meters for measuring deep currents and temperatures. A detailed description of this observational program as well as of many aspects of the monsoon circulation in this part of the Indian Ocean has been given by Schott et al. (1997), Schott and Fischer (2000), and Dengler et al. (2002). Here we use data obtained from the moorings K17-K21 deployed in the central Somali Basin between 7°N and 9°N as well as 53°E and 56°E. They were part of a triangular set-up specifically conceived to capture planetary waves propagating in this region.

The temperature records measured at the five moorings at 2000 m water depth (Fig. 3.3) showed large 30-50 days oscillations up to 0.4°C amplitude steadily increasing from July 1995 until January 1996. Given the typical stratification in the area, such temperature variability corresponds to oscillation amplitudes of the isopycnals at this depth level of about 100m. Instruments at levels higher up in the water column also showed these signals, albeit more obscured by noise. From July 1995 to February 1996 these temperature fluctuations were very similar over the mooring array, indicating the presence of larger-scale baroclinic waves. Moreover, moored records acquired at different depths indicate that strong current and temperature fluctuations are present throughout the water column, with current fluctuations as strong as 10 cm/s near the bottom.

Characteristics of the observed waves can be quantified by calculating a local dispersion relation. For our estimate, we used the time series of the meridional velocity at 400 m and 700 m water depth, and the 2000 m temperature records. We selected these data sets because they were available for at least four of the five moorings. Periods were simply calculated as the temporal interval between two successive maxima or minima in the respective time

series. Phase differences and velocities were calculated by identifying corresponding extreme values in the different time series. Once periods and phase velocities were estimated, the corresponding wavelengths were calculated.

Figure 3.4 summarizes these estimates. The fluctuation periods were smallest between July and August and increased steadily until January (Fig. 3.4a). The zonal phase velocity of the fluctuations, calculated from the K19-K21 records, was maximum in July (about 40 cm/s towards the west) and decreased strongly until October (about 15 cm/s; Fig. 3.4b). Such clear time-dependence cannot be identified in the evolution of the zonal wavelength, but there was also an indication of a decrease from 1000 km to 500 km in the period from July to October (Fig. 3.4c). The meridional phase velocity of the fluctuations was calculated from the whole data set obtained from K17 – K21. Since the main phase propagation was towards the west and the oscillation period changed with latitude, the errors associated with our visual estimates led to larger scatter in the resulting meridional phase velocity. Nevertheless, in general, the meridional phase velocity was directed southward, its magnitude being about 20 cm/s (Fig. 3.4d). Similar to the zonal wavelengths, the calculated meridional wavelengths ranged between 500 km and 1000 km (Fig. 3.4e).

A comparison between observed and theoretical dispersion relation that refers to freely propagating, first baroclinic mode, linear Rossby waves suggests that the observed fluctuations emerged during July and evolved toward freely propagating Rossby waves. The observed wavelengths were close to the wavelength where the maximum frequency in the theoretical dispersion relation (cut-off period) occurs. At this wavelength Rossby waves are characterized by a minimum in their zonal group velocity. Since our data suggest a general southward phase velocity (Fig. 3.4d) this corresponds to northward energy propagation.

The interesting question now, of course, concerns the generation of these waves and their possible interaction with the GW. The local concentration of the energy in the northern Somali Basin rules out remote forcing effects through the wind, as explored in earlier studies (Anderson and Rowlands 1976). Local wind fluctuations could also generate such fluctuations, but an analysis of the wind curl over the Arabian Sea failed to show such a concentration of fluctuation energy in the region.

This conclusion is consistent with a study by Sengupta et al. (2001), who found similar oceanic fluctuations using a numerical model of the Indian Ocean forced only with seasonal winds. They proposed hydrodynamic instabilities as the most likely generation mechanism. This seems reasonable, as the fluctuations develop with, but not before, the onset of the Southwest Monsoon, when the Southern Gyre and the GW are building up. A likely energy source for the fluctuations is the boundary between the Southern Gyre and the GW at around 4-5°N. Here, vertical shears of up to 3 m/s per 100 m have already been observed during relatively early stages of the monsoon (Leetmaa et al. 1982; Swallow et al. 1983). The lower boundary of this energetic layer rises from more than 100 m depth in the Southern Gyre to the surface in the transition zone to the GW and to more than 200 m in its center. The associated reversal of the meridional gradient of potential vorticity allows baroclinic instabilities to develop. Length scales of such baroclinic instabilities would then be 500 km or longer.

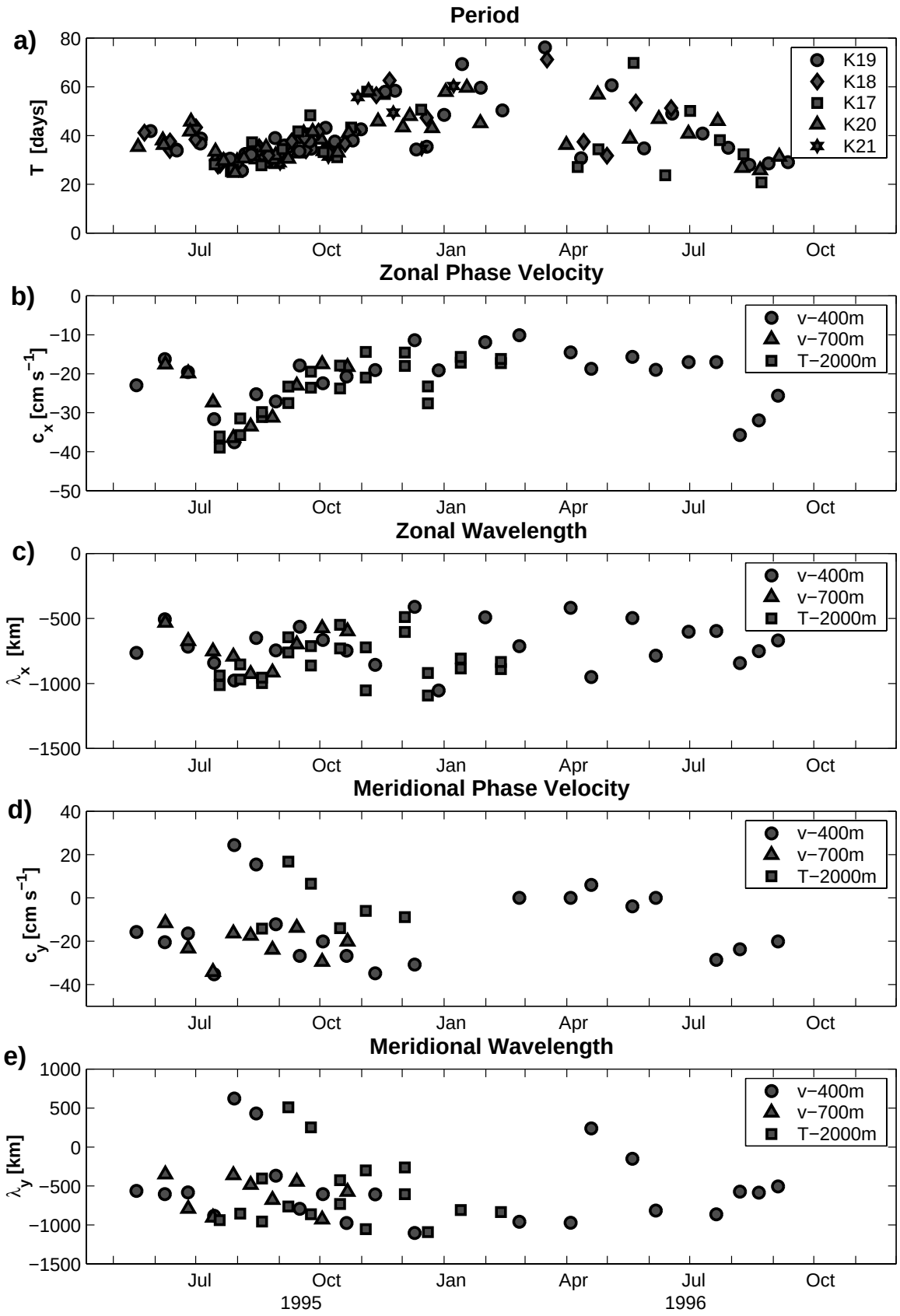

Fig. 3.4. Period (a), zonal phase velocity (b), and zonal wavelength (c), meridional phase velocity (d), and meridional wavelength (e) as calculated from meridional velocity time series at 400m and 700m water depth as well as from temperature time series at 2000 m water depth. Zonal phase velocity and zonal wavelength are calculated using data from the three moorings K19, K20, and K21. The other parameters are calculated using data from all moorings (from Brandt et al. 2003).

Likewise, the horizontal shear in this region is large, up to 4 m/s over less than 100 km, and the second meridional derivative of the zonal flow disappears in part of the domain allowing barotropic instabilities to develop. Here associated length scales would be an order of magnitude larger than the extent of the shear zone, i.e. 500 – 1000 km. Both barotropic and baroclinic instabilities are thus capable of generating current fluctuations of the observed scales, but our data do not allow us to distinguish between them. The strong nonlinearities and the closeness of the region to the equator do not allow us to apply plain linear theory. The highly variable background stratification alters the potential vorticity gradient making it deviate from the simple planetary beta. Doppler shifts due to the strong mean currents will alter the dispersion relation and it is therefore somewhat surprising how close the observed waves follow linear theory. The details of the dynamical interaction between mean and fluctuating flow cannot be resolved and quantified from the data set on hand, and an answer might only be found using high resolution numerical modeling. However, the analysis of the 8-year altimetric dataset shows strong interannual variability of the intraseasonal fluctuations, which are possibly related to the GW dynamics and in particular to its decay or collapse. A numerical study showed that besides the external forcing, the chaotic nature of the ocean dynamics contribute substantially to the interannual variability in the southwestern Arabian Sea (Wirth et al. 2002).

3.2 Eddy kinetic energy in the Labrador Sea

The Labrador Sea is a region of great interest because of its role in water mass formation, thermohaline circulation, and possibly climate change. It is one of the few sites of the World Ocean where open-ocean convection occurs, occasionally reaching great depths. Open-ocean convection sites are characterized by a cyclonic circulation, weak stratification in the interior, and the associated rising of isopycnals in the center (Marshall and Schott 1999). The cyclonic gyre in the Labrador Sea includes the West Greenland Current (WGC) flowing northwestward and the Labrador Current (LC), which flows southeastward. The WGC is mainly fed by the East Greenland Current (EGC) that involves two branches: the classical shallow EGC branch over the shelf with colder temperatures, and an offshore branch over the shelf edge with relatively warm temperatures (e.g., Fratantoni 2001; Cuny et al. 2002). This offshore flow of relatively warm water into the Labrador Sea consists of Irminger Sea Water that has its origin in waters of the North Atlantic Current (NAC). It follows the cyclonic pathways of the boundary currents within the Labrador Sea (Marshall and Schott 1999). Recently, evidence for an anticyclonic recirculation offshore of the cyclonic boundary current system has been presented through which warmer and saltier water from the NAC is carried into the Labrador Sea (Lavender et al. 2000; Fischer and Schott 2002; Fischer et al. 2004). This process may contribute a previously unknown mechanism by which the stratification of the Labrador Sea is maintained and reestablished after a convection winter. In addition to the boundary currents, a slow crossover flow that connects Greenland and Labrador across the deep Labrador Sea was observed in surface drifter and profiling float data (Cuny et al. 2002).

During the winter season, strong buoyancy loss associated with the meteorological conditions causes deep convection in the Labrador Sea that can reach depths greater than 2000 m (Lazier 1973; 1988). In recent years, strong interannual variability of convection intensity has been observed. Intense convection was observed from hydrographic sections across the central Labrador Sea in the early 1990s followed by a multi-year restratification (Lazier et al. 2002). During the latter phase moored observations showed only weak or moderate convection. In fact, the convection that was observed for the winters 1996 to 1999 (i.e. the winters 1995/96 to 1998/99) reached only maximum mixed layer depths of about 1500 m (Pickart et al. 2002; Lilly et al. 2003) and was thus not able to significantly renew the deeper LSW. This

moderate convection persisted at least until the winter 2001 and led to the formation of a shallow convective water mass, the upper LSW, that increasingly filled the upper levels of the central Labrador Sea (Stramma et al. 2004b). The interannual variability in the convection depth was not explainable in terms of the winter-to-winter variability of the local air-sea fluxes alone. Instead, lateral fluxes transporting heat and salt from the boundaries into the central Labrador Sea are needed (Lazier et al. 2002). In this exchange, mesoscale eddies are presumed to play an essential role. However, first estimates obtained from satellite altimetry indicate that only 25% to 30% of the needed lateral fluxes are carried by the observed eddies (Lilly et al. 2003). There are at least two possible mechanisms by which eddies may be generated in the Labrador Sea: first mesoscale eddies can be generated by the collapse of the convective regime at the end of the convective season (Marshall and Schott 1999) and second by the instability of the boundary current system (Heywood et al. 1994). The second mechanism seems to be dominant in the Labrador Sea. Lilly et al. (2003), by analyzing TOPEX/Poseidon altimeter and in-situ data, showed a periodic generation of coherent eddies in the WGC that propagate into the central Labrador Sea. Prater (2002), analyzing different data sets, suggested that the seasonal variability of the EKE is primarily caused by seasonal variations of the strength and stability of the WGC.

Besides the variability of the density field, the variability of the wind curl field is known to be able to change the strength of the WGC. Greatbatch and Goulding (1989) found a barotropic response of the WGC to a seasonally varying wind curl, while Spall and Pickart (2003) suggested also a baroclinic response of the circulation to variations in the wind stress curl but mainly on longer time scales. Eden and Böning (2002), using a general circulation model, showed that the main source of the simulated EKE in the Labrador Sea is barotropic instability of the WGC. Here, we derive monthly fields of gridded EKE by using along-track SSH data acquired from TOPEX/Poseidon and ERS satellites and by applying a correction with respect to the dependence of the obtained EKE on significant wave height. Using corrected EKE fields, we then focus on its temporal and spatial variability in the subpolar North Atlantic and the Labrador Sea.

The mean EKE field (Fig. 3.5) is in general agreement with results previously obtained (e.g., Fratantoni 2001; Reverdin et al. 2003; Lilly et al. 2003). It shows higher levels associated with the main currents in the region. The most prominent feature in the mean EKE field is the Northwest Corner of the NAC east of Newfoundland with maximum mean EKE value of about 1400 cm^2/s^2. In the Labrador Sea, there is a conspicuous permanent EKE maximum off southwest Greenland as well as a band of increased EKE along the LC in the southern Labrador Sea as it was very similarly found by Lilly et al. (2003) who studied TOPEX/Poseidon data of the period 1994-2000. Prater (2002) analyzed the standard deviation of TOPEX/Poseidon SSH anomaly and found besides the peak off southwest Greenland a peak in the central Labrador Sea at 58°N, 52°W. This peak can also be found in the presented EKE distribution but having only about 100 cm^2/s^2 higher levels than the background noise.

EKE time series of the WGC region (60.5-64°N, 48-53°W) and of the central Labrador Sea (56-59°N, 48-53°W, used boxes see also Fig. 3.5) are calculated by spatial averaging gridded monthly EKE values (Fig. 3.6). The complete time series from 1993-2001 is calculated using TOPEX/Poseidon data alone. In general, there is good agreement of the time series 1997-2001 from merged TOPEX/Poseidon and ERS data with TOPEX/Poseidon data alone. While the variability agrees quite well, there seems to be a slight mean offset in the central Labrador Sea between merged data and TOPEX/Poseidon data alone that possibly results from differences in the statistical dependence of the EKE on the SWH. For the description of the interannual variability of the eddy field we will use the time series calculated from TOPEX/Poseidon data alone.

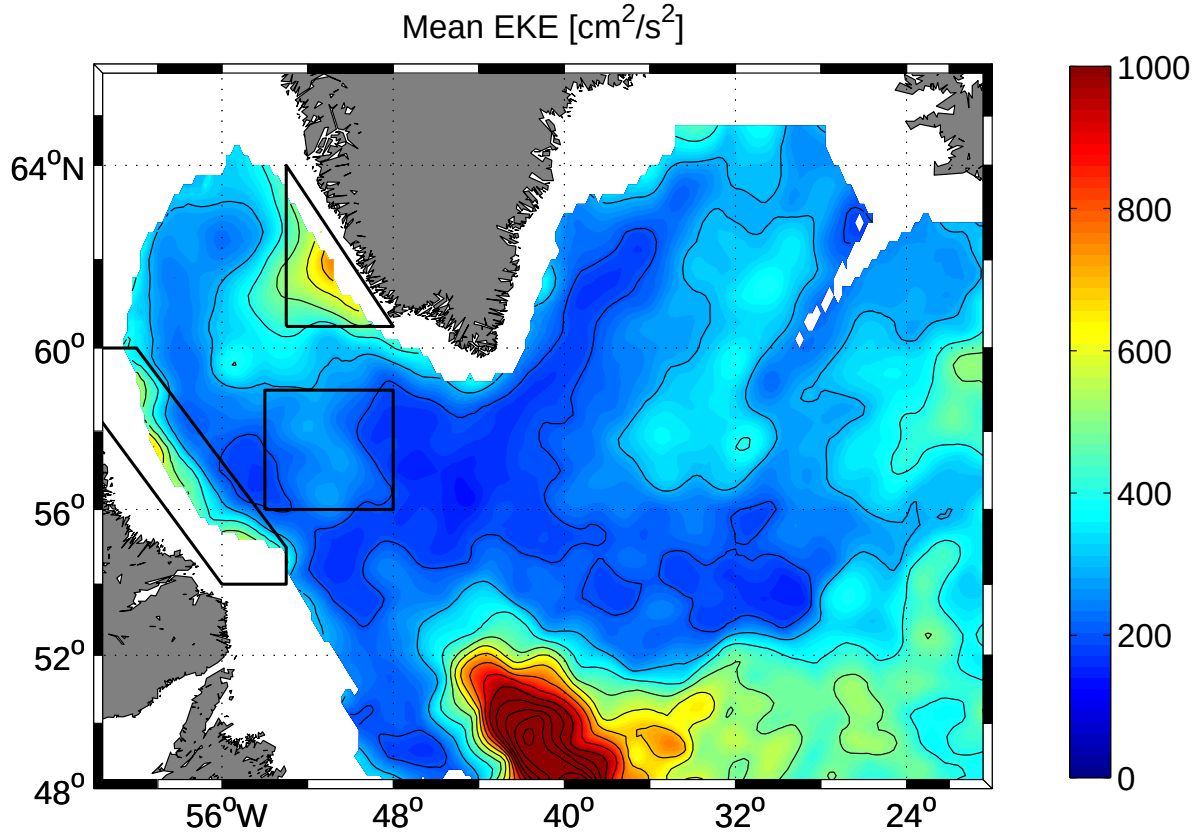

Fig. 3.5. Mean EKE distribution [cm^2/s^2] from merged TOPEX/Poseidon and ERS data for the period 1997-2001. The spacing of the contour levels is 100 cm^2/s^2. Also included are three boxes that represent the WGC region, the central Labrador Sea, and the LC region (from Brandt et al. 2004b).

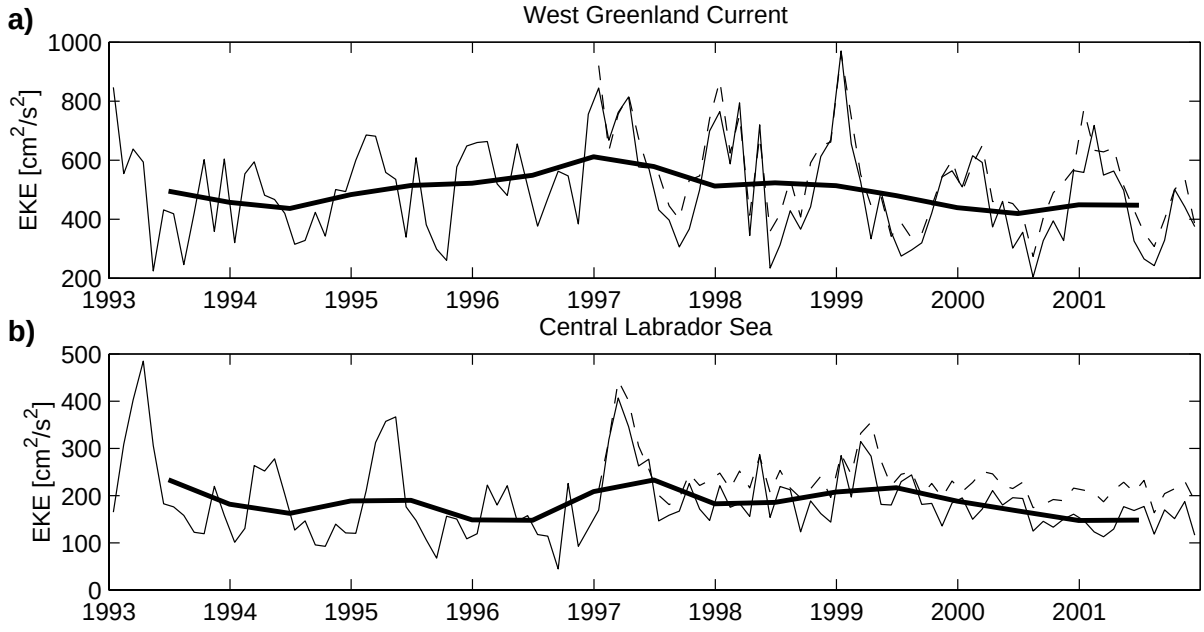

Fig. 3.6. Time series of EKE averaged for the WGC region (a) and the central Labrador Sea (b) from merged TOPEX/Poseidon and ERS data for the period 1997-2001 (dashed line) and from TOPEX/Poseidon data alone for the period 1993-2001 (thin solid line). Also included are six month overlapping annual averages (thick solid line) of TOPEX/Poseidon data alone. The two boxes are marked in Fig. 3.5 (from Brandt et al. 2004b).

The EKE in the WGC is on average more than 300 cm^2/s^2 higher than in the central Labrador Sea (Fig. 3.6). While the mean annual cycle of the WGC EKE peaks in January, within the central Labrador Sea the EKE peaks later in the year. Beside the seasonal variability, the time series show strong interannual variability. The early winter maxima of the WGC EKE are largest during 1993 as well as 1997 to 1999. The maximum annual average of the EKE is found in the year beginning in summer 1996, while local minima are found during 1994 and 2000. The interannual variability in the central Labrador Sea is quite different from that in the WGC region. In the central Labrador Sea, peaks of maximum EKE are obtained during March/April 1993-1997, except 1996.

A detailed view on the space-time evolution of the EKE in the Labrador Sea during different winters between 1993 and 2001 is given in Fig. 3.7. From 1994-1996 the annual cycle in the WGC north of 61°N was weak. Nevertheless, there were considerably high EKE levels throughout the whole period indicating a more continuous generation of EKE in the WGC. These years were characterized by the presence of large volumes of deep LSW associated with a doming of the isopycnals in the central Labrador Sea (Lazier et al. 2002). A possible increase in the horizontal density gradients related to this doming could have led to an increased strength of the WGC and thus to the observed more continuous EKE generation. However, from 1997-2001 we observed a strong annual cycle in the WGC EKE generation, with maximum values during January and particularly strong minima during summer. This period is characterized by the increasing formation of lighter, upper LSW (Lazier et al. 2002; Stramma et al. 2004b). In this case the smaller horizontal density gradient could have led to a decreased strength of the WGC. The observed strong annual cycle may be explained by the annual cycle of the wind stress curl forcing the WGC to switch between more stable and unstable phases.

The propagation characteristics of the altimetrically estimated EKE indicates a slow propagation of the WGC EKE into the central Labrador Sea during 1997-2001 with about 3 cm/s. From mooring data, Lilly et al. (2003) identified the associated eddies that occurred in the central Labrador Sea after mid-1997, as predominantly buoyant, long-lived anticyclones transporting warmer and saltier Irminger Sea Water into the central Labrador Sea. This situation is well presented in a recent model study by Eden and Böning (2002) who demonstrated the importance of the WGC as eddy shedding regime sending mostly anticyclonic eddies into the central Labrador Sea that are generated by the barotropic instability of the boundary current.

An almost simultaneous increase of the EKE during March/April in the central Labrador Sea between 56°N and 60°N can instead be observed during 1993-1995 and 1997. The three years 1993-1995 are characterized by deep convection associated with the renewal of deep LSW (Lilly et al. 2003). From mooring data, Lilly et al. (2003) revealed the existence of short-lived "convective lenses" predominantly during these years that were identified as originating in the central Labrador Sea during deep convection. The observations of short-lived eddies correspond to the rapid destruction of EKE in the central Labrador Sea that is observed in the altimeter data.

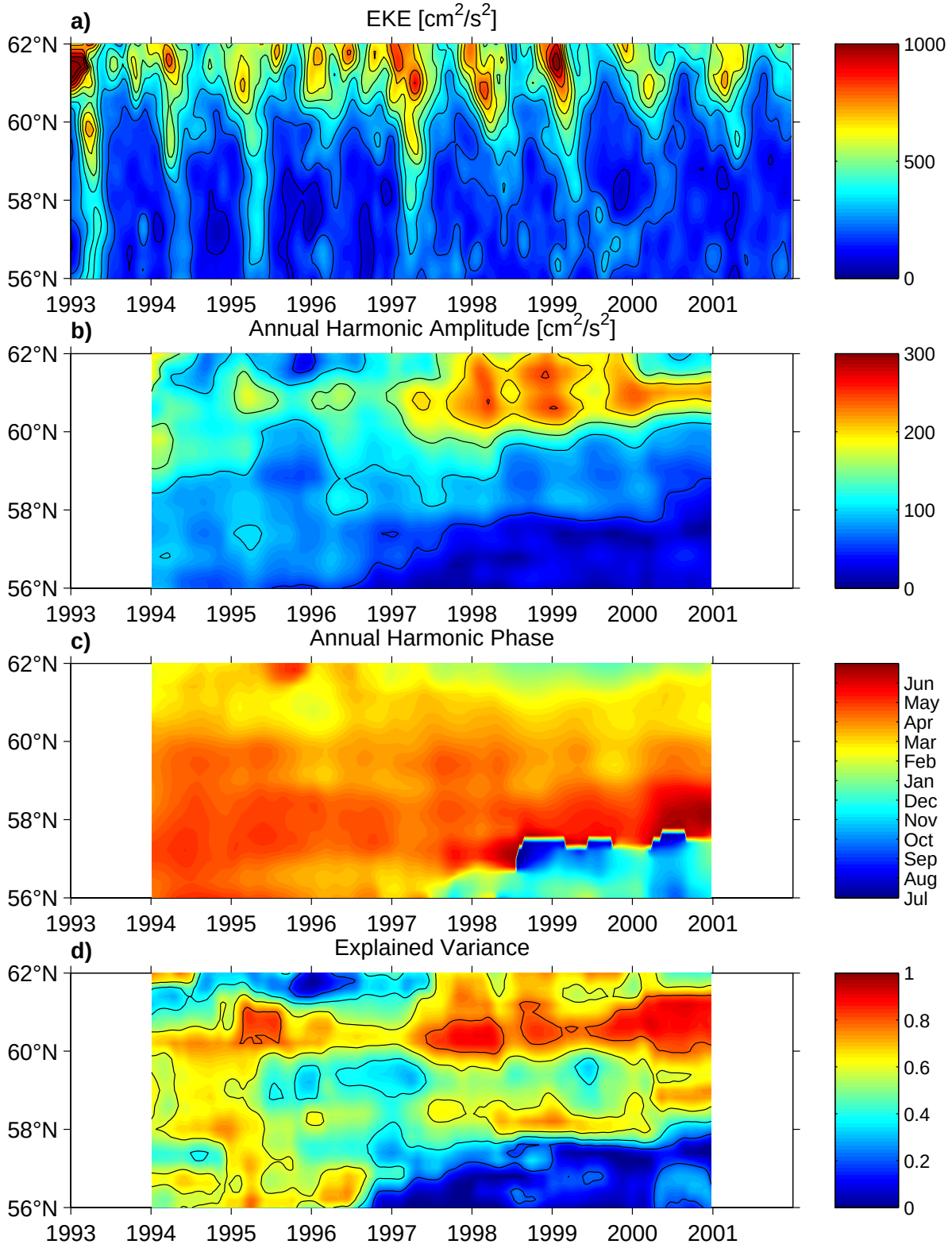

Fig. 3.7. (a) Latitude-time diagram of EKE in the Labrador Sea averaged between 48°W and 54°W from TOPEX/Poseidon data alone for the period 1993-2001 as well as (b) amplitude [cm^2/s^2], (c) phase (month of maximum EKE), and (d) explained variance of the annual harmonic of the EKE as calculated from two-years long segments. Note the almost instantaneous generation of EKE in the central Labrador Sea (between 56°N and 59°N) during April/March 1993-1997, except 1996, combined with its fast destruction during the summer 1993-1995 and the maintenance of increased EKE levels in the central Labrador Sea during 1997-2000 (from Brandt et al. 2004b).

The winter 1997 that is characterized by the interannual WGC EKE maximum (Fig. 3.6) seems to mark the transition between both states described above. During January 1997 large EKE levels were observed in the WGC region that propagate away from the source region. However, during March 1997 an instantaneous increase of the EKE is observed in the whole central Labrador Sea that cannot be explained by the eddy propagation from the WGC (Fig. 3.7). In particular, during March 1997 a band of enhanced EKE can be identified reaching from 54°W, 59°N to 48°W, 56°N (Fig. 3.8). This band marks the northern boundary of the convective patch as observed during that winter from profiling float data by Lavender et al. (2002). From a hydrographic section taken during March 1997 (Pickart et al. 2002) the extension of the convective patch can be estimated by the outcropping of the isopycnal σ_θ = 27.75 kg/m^3, which marks the upper bound of the LSW (white bar in Fig. 3.8). Following the hydrographic section toward north, buoyant water originating in the WGC was observed near the surface that prevented deep convection in this region from. However, the region north of the convective patch that is associated with an increased horizontal density gradient coincides with the band of enhanced EKE observed with altimetry. The southern boundary of the convective patch may be the LC that was also associated with an increased EKE level during March 1997. After the fast destruction of the "convective lenses", the remaining EKE during June 1997 may correspond to the long-lived anticyclones observed by Lilly et al. (2003) in mooring data that are generated in the WGC region some months before. In spite of strong surface heat fluxes during February/March 1997, the winter 1997 was moderate with respect to atmospheric forcing and resulted in moderate convection reaching down to 1500 m water depth (Labseagroup 1998; Pickart et al. 2002). Nevertheless, the observed behavior of the EKE field during that winter is in general agreement with the scheme given by Marshall and Schott (1999), in which the collapse of the convective regime at the end of the convective season is associated with baroclinic instabilities leading to enhanced EKE levels. The winter 1997 may thus be seen as an exemplar case for the evolution of EKE that is largely generated near the convective patch in the central Labrador Sea.

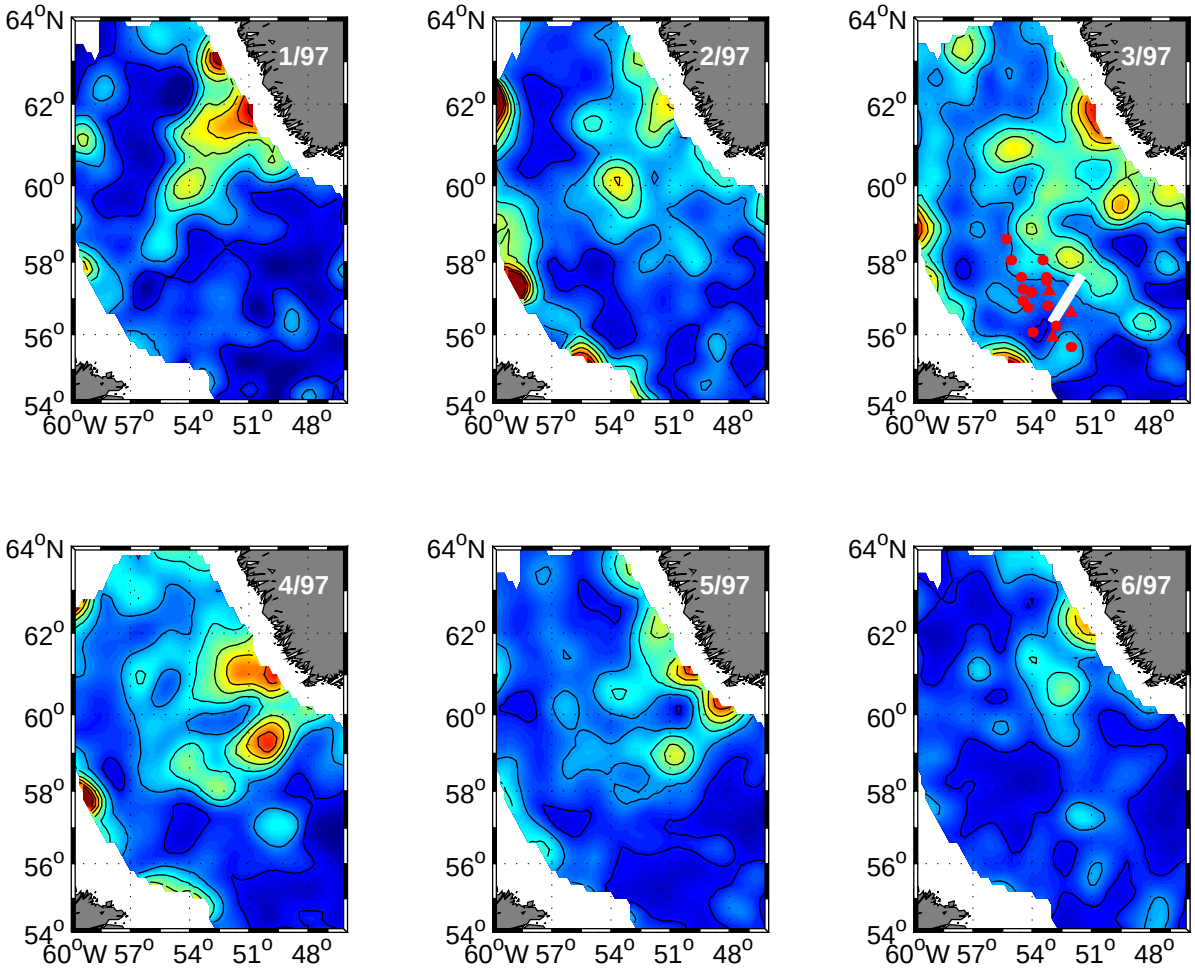

Fig. 3.8. Monthly mean EKE in the Labrador Sea for the period January to June 1997 from merged TOPEX/Poseidon and ERS data. The contour levels are spaced by 200 cm^2/s^2. The locations of mixed layer depths between 800 and 1000m (red circles) and between 1000 and 1350m (red triangles) from profiling floats measurements between November 1996 and April 1997 (Lavender et al. 2002) are given in the March 1997 subplot as well as the location of moderate convection that is determined from a hydrographic section taken during March 1997 as being the region bounded by the outcrop positions of the isopycnal surface σ_θ = 27.75 kg/m^2 (white bar) (Pickart et al. 2002) (from Brandt et al. 2004b).

4 Internal Solitary Waves and Strait Dynamics

4.1 Internal Solitary Waves in the tropical Western Atlantic

Large-amplitude internal solitary waves propagating along the near-surface waveguide over long distances are frequently observed in the World Ocean (Ostrovsky and Stepanyants 1989, Apel et al. 1995). They mainly arise from the disintegration of the internal tides generated by the interaction of a barotropic tidal flow with topographic features like, e. g., continental slopes (e.g., MacKinnon and Gregg 2003; Moum et al. 2003) or strait sills (e.g., Brandt et al. 1996 1997 1999a). As internal solitary waves can be linked to different phenomena occurring within the water column like, e. g., variations in water velocity, salinity, temperature, or in passive tracer concentration, or at the sea surface like, e. g., modulation of the surface wave spectrum (Brandt et al. 1999b), surface wave breaking, or accumulation of surfactants, different measurement techniques can be employed for their detection. With the advent of satellite remote sensing, the existence of tidally induced internal waves, often ranked in trains of internal solitary waves, was revealed in the entire World Ocean. The acknowledgment of the ubiquity of tidally induced internal waves, mainly achieved through satellite observations, suggests that these oceanic features exert a significant contribution to the dissipation of the rotational energy of the Earth-Moon system and to the local mixing of different water masses in the ocean (Munk and Wunsch 1998; MacKinnon and Gregg 2003; Moum et al. 2003).

Here we report on observations of large-amplitude, pulse-like internal solitary waves in the region occupied by the North Equatorial Counter Current (NECC) in the tropical Atlantic Ocean and discuss their behavior in comparison to the typical behavior of trains of tidally generated internal solitary waves in the World Ocean. The data used are high-resolution velocity data, which were acquired with a 75 KHz phased-array acoustic Doppler current profiler (ADCP) named Ocean Surveyor (OS), during the RV *Sonne* cruise 151 (SO151) in November 2000. The measurement of highly accurate currents requires precise navigation and heading data that were supplied from a differential GPS and an Ashtech 3D GPS receiver (Fischer et al. 2003). Due to calm weather the vessel was very stable and we estimated that the one-minute low-pass filtered horizontal velocity was measured with an accuracy better than 0.04 m/s.

Fig. 4.1 shows the northward (Fig. 4.1a) as well as the eastward (Fig. 4.1b) component of the horizontal velocity field (the data represent averages between 30 m and 78 m) as measured by the OS on November 12 2000 along a meridional section at 44°W. Between about 3.5°N and 6°N strong eastward current velocities were detected, which are associated with the NECC. A maximum core velocity of about 1.8 m/s was observed at about 5.1°N. In general, the observed velocity field shows undulations with length scales of O(100 km). Superimposed on these undulations are several small-scale, pulse-like disturbances. In particular, within the region occupied by the NECC, three sharp, well-distinguished peaks are evident in both velocity components. These are located about 70 km apart, the northernmost one being located at about 5.9°N. Assuming that the Coriolis force can be neglected on the length scales characterizing the observed disturbances, the wave propagation direction is given by the direction of maximum horizontal velocity anomaly. For all three waves, this direction is about north-north-east and therefore strongly inclined (about 60 to 65 deg) with respect to the main axis of the NECC, which flows eastward.

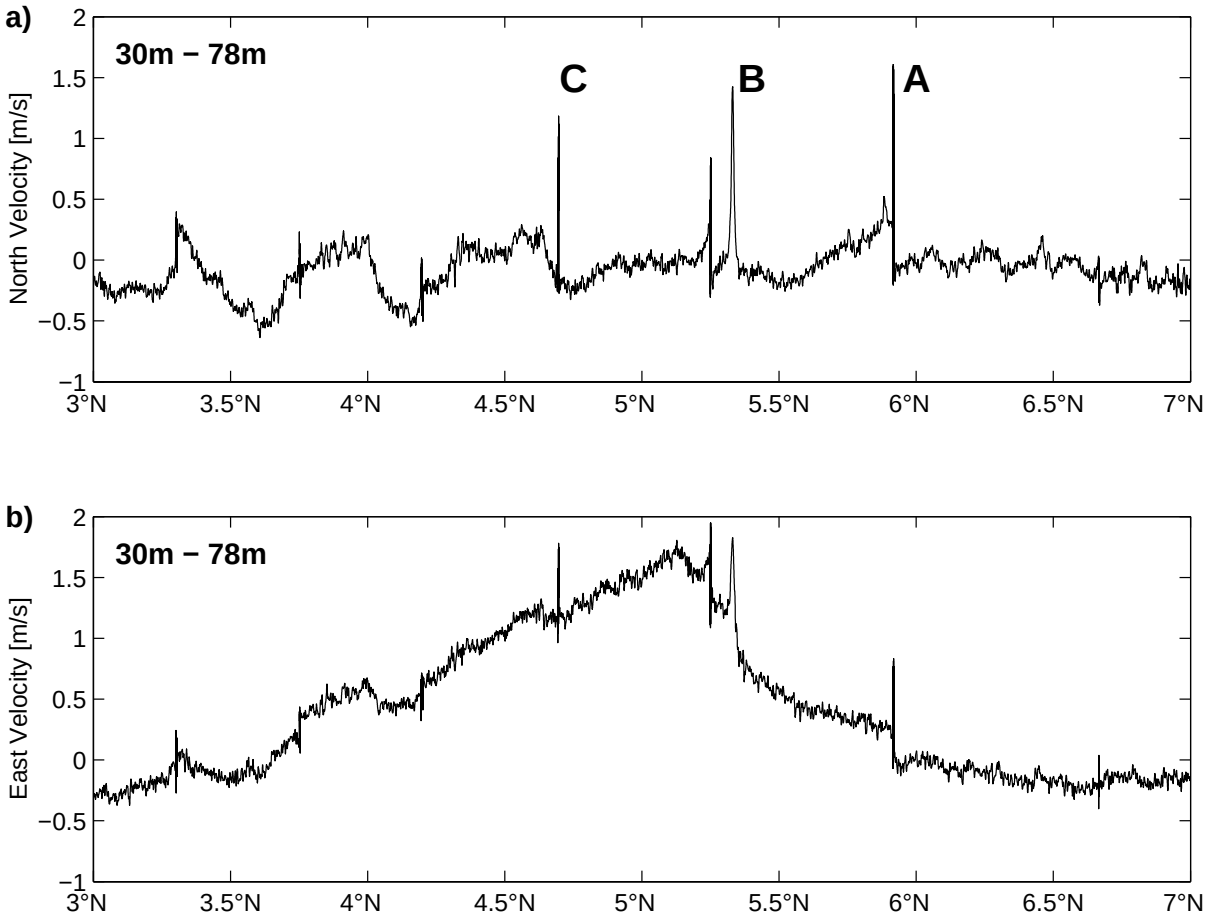

Fig. 4.1. Northward (a) as well as eastward (b) component of the horizontal velocity field as measured by the OS on November 12 2000 at 44°W as function of latitude. The data represent one-minute low-pass filtered velocity data averaged between 30 m and 78 m depth. The three large-amplitude waves discussed in the following sections are marked by A, B, and C (from Brandt et al. 2002b).

While the vessel passed through the three waves, sharply defined bands of increased surface roughness with breaking surface waves were observed visually, which also led to strong signals on the ship radar. A detailed view of the horizontal as well as of the vertical velocity structure within the three disturbances is presented in Fig. 4.2, in which the velocity data are plotted as function of time. The Doppler shift inherent in the observed data was estimated using the (known) ship velocity as well as an estimate of the phase velocity (2.5 m/s). The northward components of the horizontal velocity field associated with the three waves are very similar in strength and structure. On the contrary, the eastward components are quite different. In particular wave **A** marks a transition region between NECC and undisturbed ocean: While in front of wave **A** (north of it) the eastward velocity is about zero, this velocity is significantly larger (about 0.2 m/s averaged between 30 and 78 m, see also Fig. 4.1) in its rear (south of it). Wave **B** is located entirely within the NECC, but it also marks, like in the previous case, a transition region. In front of wave **B** smaller eastward velocities (about 0.8 m/s averaged between 30 and 78 m, see also Fig. 4.1) are encountered than in its rear (about 1.2 m/s, see also Fig. 1). The thickness of the NECC is at maximum in the region occupied by wave **C**. There, eastward velocities larger than 1 m/s are encountered in the upper 120 m of the water column. Note that in the eastward as well as in the vertical component of the velocity fields the maximum anomalies associated with the internal waves deepen from wave **A** to wave **C**. As stressed before this behavior cannot be detected in the northward component of the velocity field.

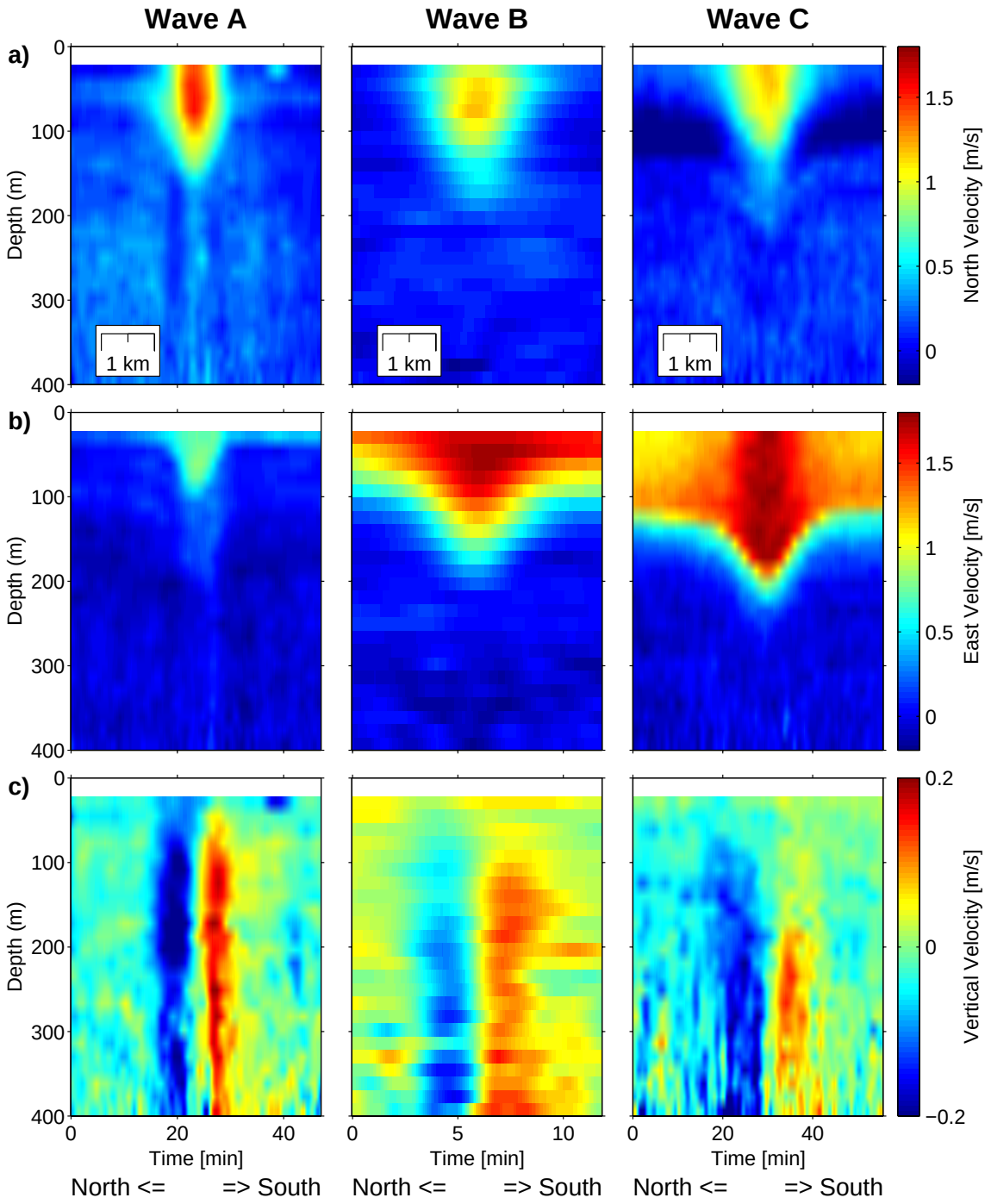

Fig. 4.2. Northward (a), eastward (b), and vertical (c) component of the velocity field for the three waves A, B, and C as function of time and depth. The horizontal length scales given in (a) were obtained by estimating the Doppler shift inherent in the observed data from the known ship velocity as well as from an estimate of the phase velocity (from Brandt et al. 2002b).

The horizontal as well as the vertical velocity fields of each wave show the typical structure associated with internal gravitational solitary waves. The shapes of the isolines of the northward velocity component (or, equivalently, of the horizontal velocity anomalies) are in fact nearly semi-elliptical and the shapes of the isolines of the vertical velocity component nearly antisymmetric. The front of each waves is associated with downward velocity, the rear with upward velocity, their maximum amplitude being about 20 cm/s. These characteristics of the observed features agree qualitatively with those of large-amplitude internal solitary waves described theoretically and observed in high-resolution measurements (see, e.g., Vlasenko et al. 2000).

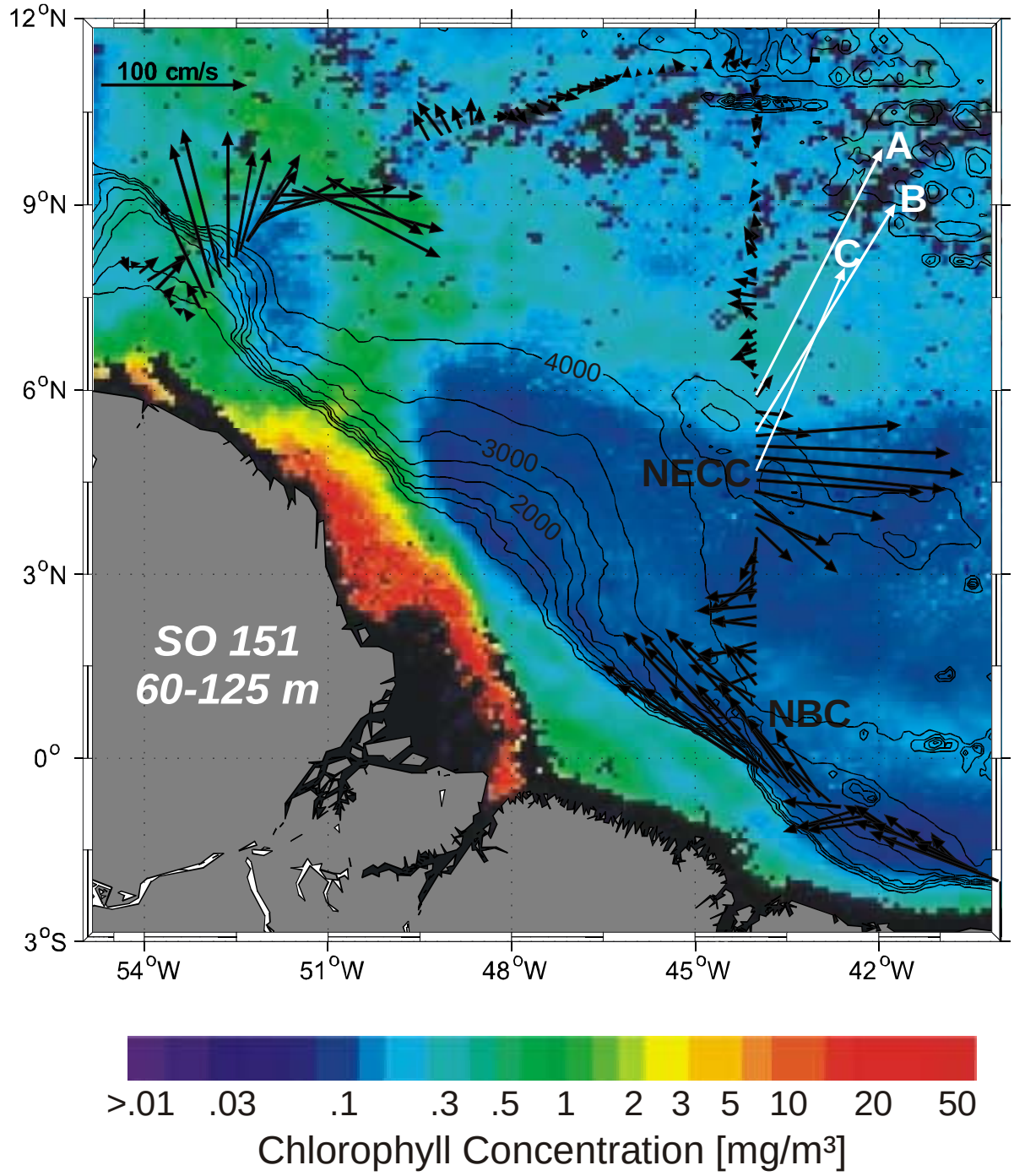

Fig. 4.3. Geographical map of the western tropical Atlantic including the NBC/NECC retroflection zone with the near-surface current vectors (the data are averaged between 60 and 125 m depth) measured during RV Sonne cruise SO151 superimposed on chlorophyll concentration measured by the SeaWifS sensor aboard the SeaStar satellite. The white arrows refer to the maximum velocity anomalies associated to waves marked by A, B, and C in Fig. 4.1 (from Brandt et al. 2002b).

An overview of the shallow current branches in the NBC/NECC retroflection zone (the data refer to averages between 60 and 125 m depth) superimposed on the chlorophyll concentration observed by the SeaWiFS sensor aboard the SeaStar satellite during November 2000 is given in Fig. 4.3. In particular, using the data acquired along two sections oriented almost perpendicular to the coast that merge at the Mid-Atlantic Ridge, the structure of the NBC retroflection can be elucidated. At 44°W the NBC is mainly confined to the local steep shelf break, its maximum velocity being about 1 m/s. Note, however, that somewhat weaker flow extends offshore over nearly 300 km distance. Further northwest, off French

Guyana (near 53°W), the currents at the shelf break turn offshore and then eastward at about 9°N. However, the chlorophyll distribution reveals that the change in the observed current direction represents an eddy released by the NBC. As discussed before, at 44°W we observed a fully developed NECC in the latitude band from 3.5°N to about 6°N.

In Fig. 4.3 the maximum velocity anomalies associated with the three large-amplitude internal solitary waves described in the previous section are also shown. The waves propagate toward north-north-east, in a region of large water depths (even in the region characterized by the topographic variations associated with the Sierra Rise the water depth exceeds 3000 m). Assuming that they were generated at the steep Brazilian shelf break (which could be compatible with a tidal generation mechanism) they should have traveled about 500 km to reach the location where they were observed. Despite the lack of topographic constrictions in the region, which could allow for wave energy focusing, the tidal generation mechanisms along the Brazilian continental shelf (i.e., a line source mechanism) could be still effective in producing large-amplitude internal solitary waves, especially if the waves are amplified by wave-current interaction occurring across frontal regions with strong horizontal density gradients (Kuznetsov et al. 1984). The fact that such a mechanism can be efficient in equatorial regions is confirmed by Pinkel (2000), who observed tidally generated internal solitary waves in the western equatorial Pacific Ocean. However, in contrast to our measurements, the trains of solitary waves he observed were clearly composed of rank-ordered elements and the peak velocities of the single waves were much smaller (about 80 cm/s).

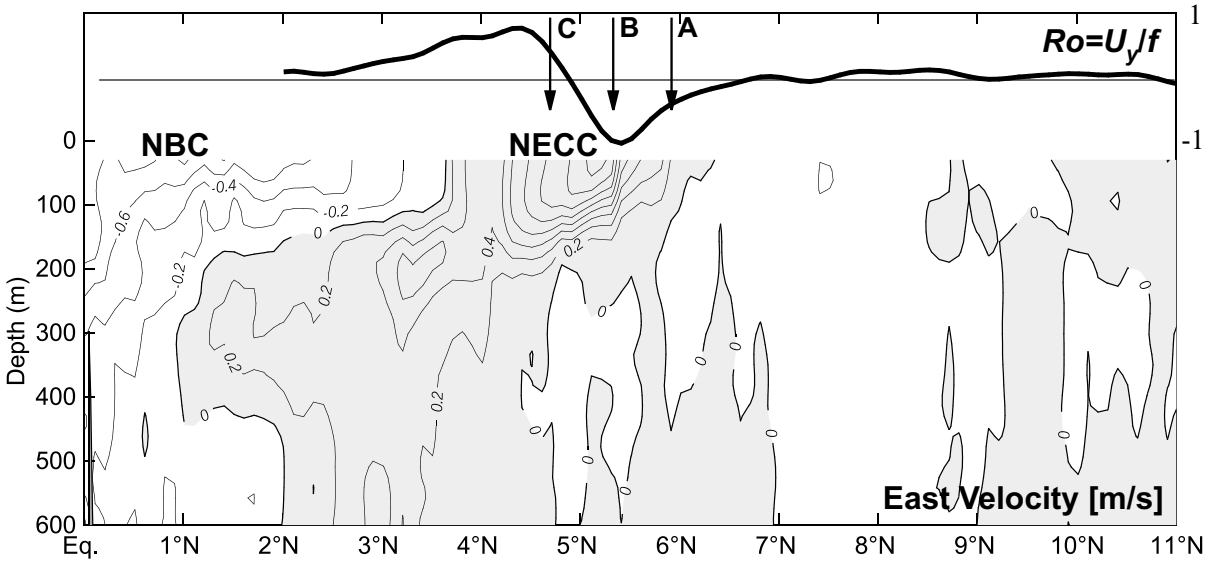

Fig. 4.4. Eastward component of the velocity field as function of latitude and depth. A local Rossby number (thick solid line) as well as the positions of waves A, B, and C (see Fig. 4.1) is shown above the contoured isotachs (from Brandt et al. 2002b).

In Fig. 4.4 the eastward component of the current field associated with the NECC is depicted. The velocity data were interpolated onto a regular grid by objective mapping using horizontal scales of 10 km and vertical scales of 40 m. Thus, the currents appear much smoother than in the original resolution. Nevertheless, the eastward flowing NECC centered at 5.1°N still shows 1.6 m/s currents near the surface. Large horizontal and vertical shears are associated with this current. To assess the nonlinearity inherent in this jet, the relative vorticity estimated by the zonal variation of the eastward velocity component $\partial U/\partial y$ scaled by the planetary vorticity f is shown above the contoured isotachs. Note that for this calculation, the flow (averaged between 60 and 125 m depth) was filtered over a 100 km length scale. This quantity can be interpreted as a local Rossby Number and, because it is

close to unity at both sides of the jet, it indicates that the NECC has a large ageostrophic component. In conclusion, aspects of the behavior of the internal solitary waves observed in the NECC strongly differ from that typically observed for trains of tidally generated internal solitary waves. This, though not excluding that they are of tidal origin (as their separation distance would suggest), indicates that different mechanisms were possibly involved in their generation and/or evolution. Moreover, these waves may play an important role in mixing processes within the equatorial region. In fact, Pinkel (2000) suggested by analyzing data from the western equatorial Pacific Ocean that while the intrinsic shear of the observed internal solitary waves is too small to reduce local values of the gradient Richardson number below 1/4, internal solitary waves are able to trigger instability of the background current shear in equatorial current regimes enhancing vertical mixing.

4.2 Exchange flow through the Strait of Gibraltar

Through the Strait of Gibraltar Atlantic water flows, in the near surface layer, toward the Mediterranean basin. There, this water is transformed into saltier water, which eventually leaves the Mediterranean through the same Strait in the near bottom. Changes in the water mass characteristics in the Atlantic and/or Mediterranean waters flowing through the Strait of Gibraltar, that may result from different variations in the two neighboring basins, may profoundly affect the exchange flow through the Strait of Gibraltar (Myers and Haines 2002), which contributes to observed sea level variations in the Mediterranean Sea (Ross et al. 2000). This has been partly attributed to variations in the hydraulic regime occurring in the Strait of Gibraltar, which may flip between maximal and submaximal exchange on time scales from seasonal to interannual (Garrett et al. 1990). According to the "classic" hydraulic models for the exchange flow through the Strait of Gibraltar (Farmer and Armi 1986; Bryden and Kinder 1991) maximal exchange flow is achieved when the flow is hydraulically controlled at Camarinal Sill and Tarifa Narrows, while submaximal exchange flow is achieved when it is hydraulically controlled only at Camarinal Sill. High-resolution numerical simulations of the exchange flow through the Strait of Gibraltar give a more complex picture: it is characterized by fragmented regions where the flow is hydraulically controlled, which are interrupted by regions of subcritical flow (Izquierdo et al. 2001). Moreover, this exchange flow is strongly influenced by the tides. Due to the tidal currents the control at the Camarinal Sill is periodically flooded and eastward propagating internal bores are generated that disintegrate into trains of internal solitary waves frequently observed by in-situ and remote sensing techniques (Brandt et al. 1996). Quasi-steady as well as non-steady theories predict that the exchange flow increases with tidal amplitude (Farmer and Armi 1986; Helfrich 1995; Brandt et al. 1996). Thus, a profound knowledge of the two-dimensional tidal dynamics in the Strait of Gibraltar is fundamental for the prediction of variations in the exchange flow. In the last years, different large projects have been initiated to observe extensively the temporally and spatially varying flow structure within the Strait of Gibraltar. Armi and Farmer (1988), for instance, presented experimental evidences of the existence of control points for the outflowing water at the Spartel Sill and at the Camarinal Sill and for the inflowing water at the Tarifa Narrows. During part of the observations, the control was permanent only at the Spartel Sill and at the Tarifa Narrows. According to these findings, in the frame of the hydraulic control theory, the exchange flow in the Strait of Gibraltar was thus maximal during this part of the observational period. More recently, during the CANIGO (Canary Islands Azores Gibraltar Observations) project, an attempt was made to measure the tidal flow as well as the exchange flow at different locations within the Strait.

Now, not only the existence of different theories, but also the large dataset available allows for an accurate assessment of the performance of numerical models, i.e., we can obtain

characteristics of the simulated tidal flow as well as exchange flow in the Strait of Gibraltar that are consistent with the underlying data set and with the existing theories. Once this result is achieved, these numerical models can be used to investigate the climatological sensitivity of the simulated dynamics in the Strait of Gibraltar.

The model used for this investigation is the two-dimensional, nonlinear, two-layer numerical model described by Izquierdo et al. (2001) extended to include the eastern part of the Gulf of Cadiz and the western part of the Alboran Sea. The model allows the simulation of the mean exchange as well as tidal flow in the Strait of Gibraltar. Results of the numerical model are compared with results of an inverse tidal model that represents a fit to data taken during extensive measurements at the eastern entrance of the Strait of Gibraltar (Ceuta-Algeciras section) in the frame of CANIGO (Baschek et al. 2001) as well as with different bottom pressure and tide gauge measurements and, in general, good agreement is found.

In Fig. 4.5 the mean surface and interface positions are depicted, which illustrate the mean along-strait and cross-strait pressure gradients in a central region of our model domain. The model yields a mean along-strait sea level difference of about 6 cm between the two opposite entrances of the strait. The sea level decrease toward east is, however, rather irregular, which can be, at least partly, explained as due to the upper layer flow over a variable lower layer interface. Especially in the sill region this effect is evident: a band of decreased sea level crossing the strait can be found over Camarinal Sill, where the interface strongly slopes down toward west. Across the strait, a sea level difference of about 3 cm at the western entrance and of about 9 cm at the eastern entrance is simulated, which accounts for the noticeable importance of the Coriolis force in the presence of a variable upper layer thickness and hence velocities. The opposite structure is found for the interface depth: a weak cross-strait gradient at the eastern entrance and a strong one at the western entrance are encountered there.

The time-averaged upper and lower layer along-strait velocities are depicted in Fig. 4.6. In the upper layer, large velocities (up to 0.8 m/s) are found in the eastern part of the strait, while, in the lower layer, there are several regions where values up to -0.7 m/s are encountered. These regions are located near Camarinal and Spartel sills and, together with Tarifa Narrows, correspond to regions, where the flow is hydraulically controlled (Fig. 4.7). To identify these regions, a composite Froude number defined as $G = G_1 + G_2$ was calculated, with

$$G_{1,2} = \left\langle \frac{u_{1,2}^2}{g\,\Delta\rho/\rho\,H_{1,2}} \right\rangle$$

where $u_{1,2}$ denote the upper and lower layer velocities, $H_{1,2}$ the upper and lower layer thicknesses, g the acceleration of gravity, $\Delta\rho$ the density difference between both layers, and ρ the mean density. The brackets denote a time average over the whole simulation period. The model simulates, on average, a control of the outflow at the Spartel Sill and a control of the inflow at the Camarinal Sill, while, at the Tarifa Narrows, only within an isolated region near the northern shore the inflow is hydraulically controlled. This, in the frame of the hydraulic theory, would correspond, on average, to maximal exchange flow through the Strait of Gibraltar. Note that a detailed discussion about the temporal variability of these control regimes within a tropical month can be found in Izquierdo et al. (2001).

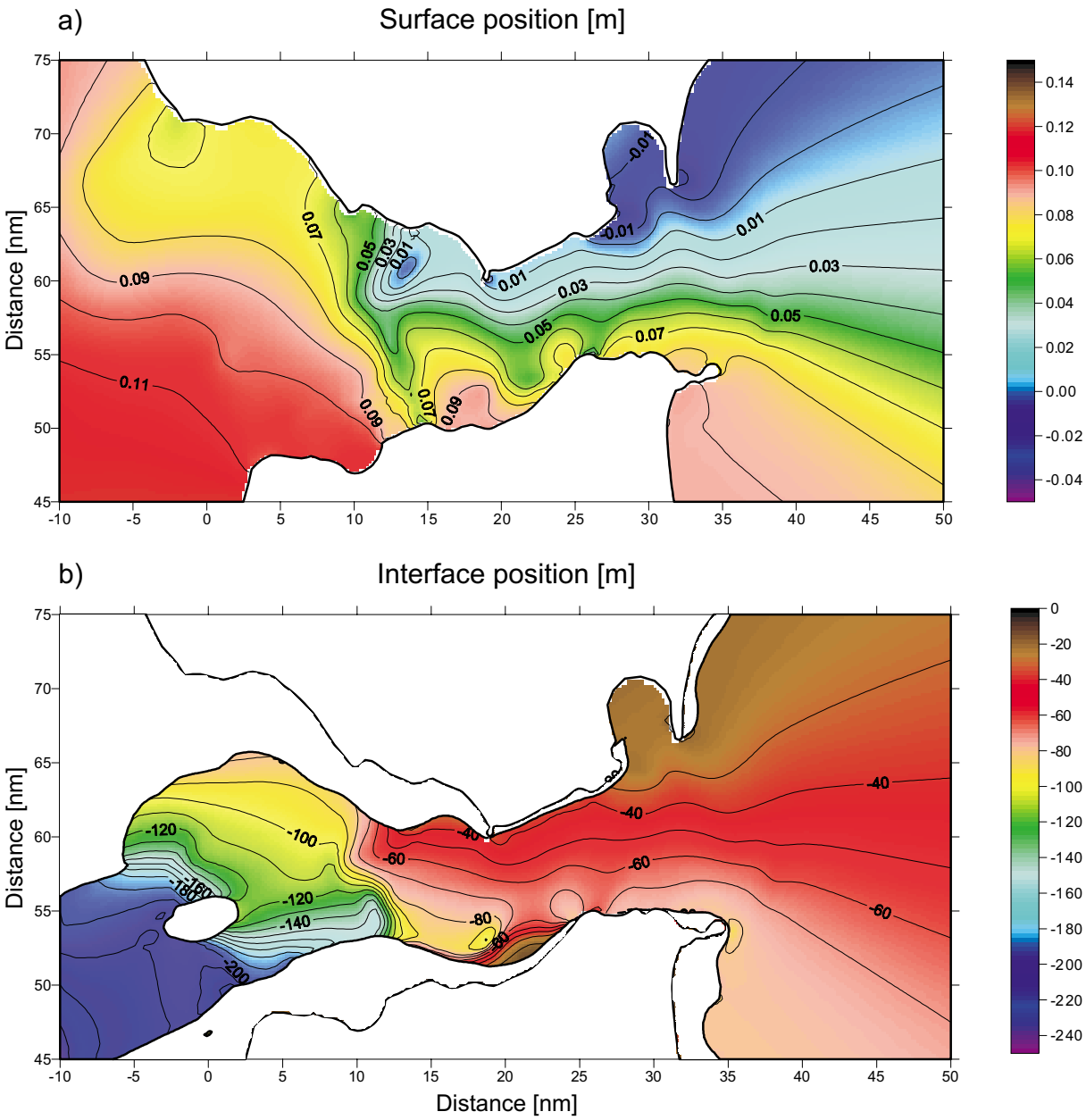

Fig. 4.5. Time-averaged sea surface (a) and interface (b) positions as simulated by our numerical model (from Brandt et al. 2004a).

We now investigate the sensitivity of the simulated exchange flow to changes in the (climatologically relevant) density difference between Atlantic and Mediterranean waters. The results of our investigation show that an increase in the density difference (i.e., an increase in the baroclinic pressure gradient and hence in the Mediterranean outflow) yields an increase in the simulated exchange flow and a decrease in the net inflow. Consider now a climatic variation, in which the density difference between Atlantic and Mediterranean waters is changed, but which does not affect the mass balance within the Mediterranean. In this case the change in the density difference must be connected with a change in the along-strait pressure gradient and hence in the sea level drop from the Atlantic to the Mediterranean in order to keep the net inflow constant. On the other hand, an abrupt change in the density difference between the two waters would result in a variation of the net inflow. As a consequence the sea level in the Mediterranean must change and eventually a new equilibrium is reached, in which the mass balance is fulfilled again.

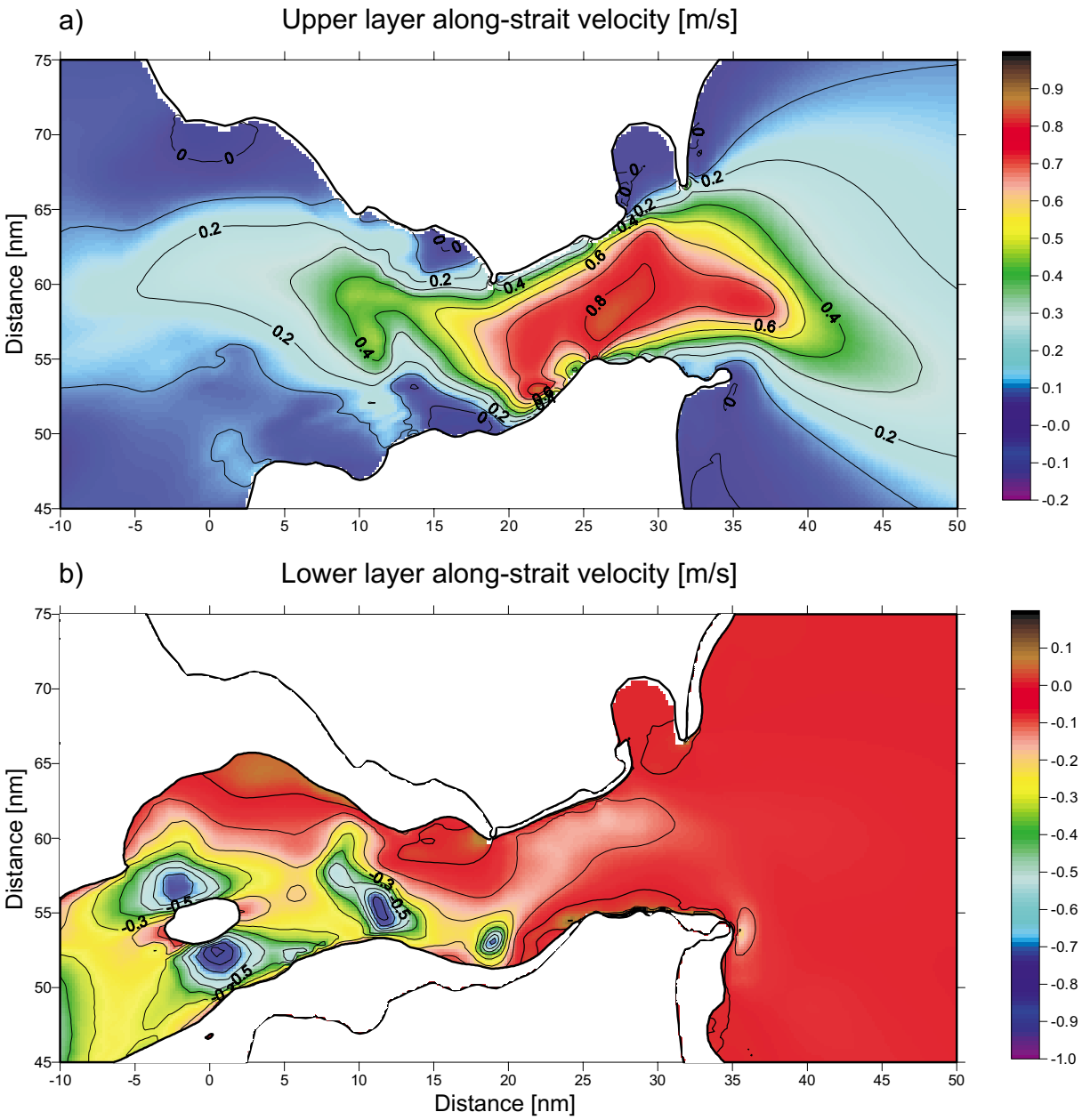

Fig. 4.6. Time-averaged upper layer (a) and lower layer (b) along-strait velocity as simulated by our numerical model (from Brandt et al. 2004a).

In our numerical model, given a certain density difference between Atlantic and Mediterranean waters, we can iteratively search for the sea level drop that yields the same net inflow as in our central experiment. To reach this goal, the iterations were performed by adding a constant offset to the fixed sea level at the Mediterranean boundary. We found that, in the case of an increased/decreased relative density difference (relative to our central experiment) of 10^{-4}, an increase/decrease of 0.73 cm in the sea level drop between Atlantic and Mediterranean yields the same net inflow as in our central experiment. Note that in the different iteration runs for a given density difference, the exchange flow (i.e. the difference between Atlantic and Mediterranean transport) remains virtually constant and that, for the considered range of density differences, we found no change in the hydraulic regime: all these simulations yield almost the same spatial distribution of control regions as depicted in Fig. 4.7.

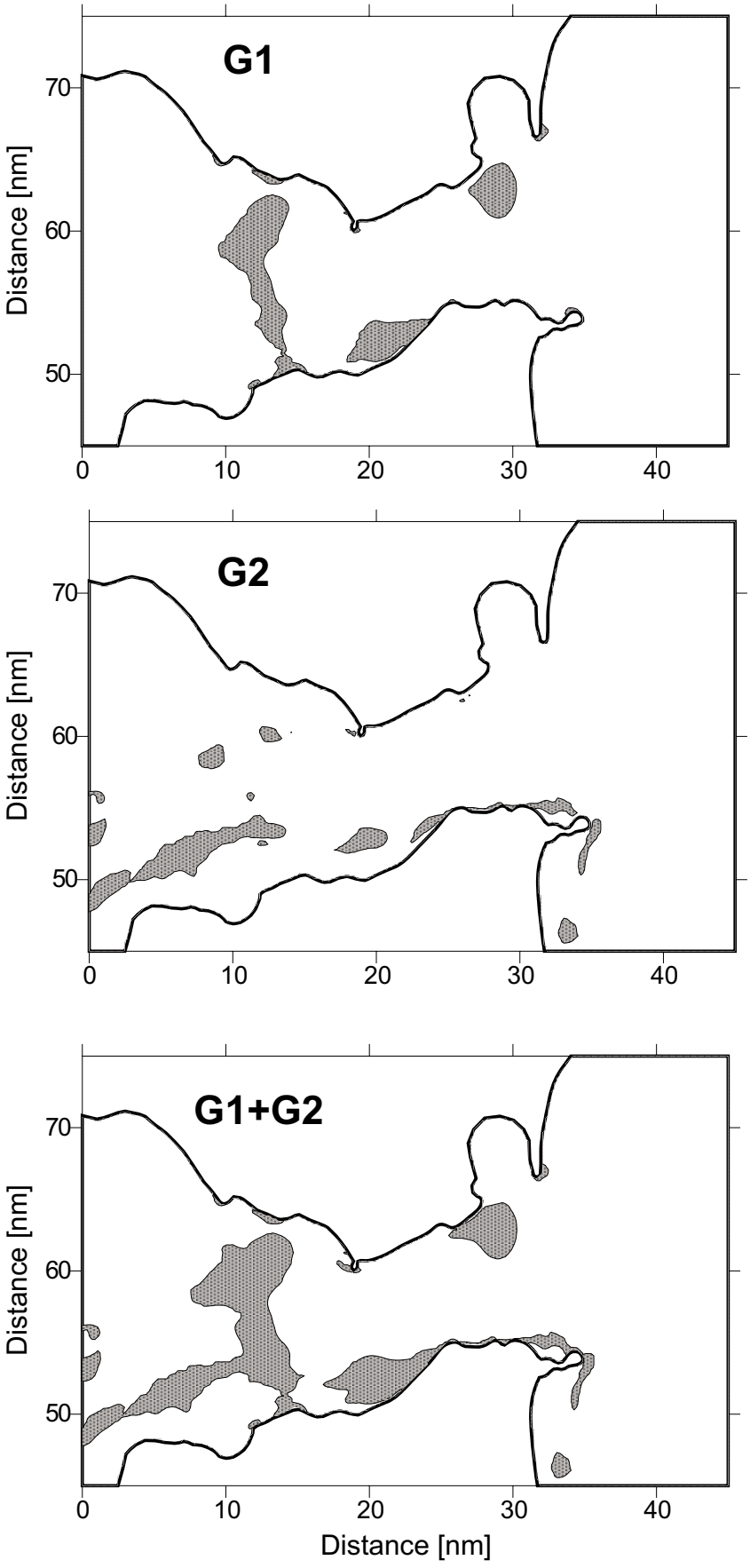

Fig. 4.7. Geographic maps of the Strait of Gibraltar with inserted regions where the time-averaged upper layer (G1), lower layer (G2) and composite Froude number (G1+G2) as simulated by our numerical model are larger than one (gray shaded patches) (from Brandt et al. 2004a).

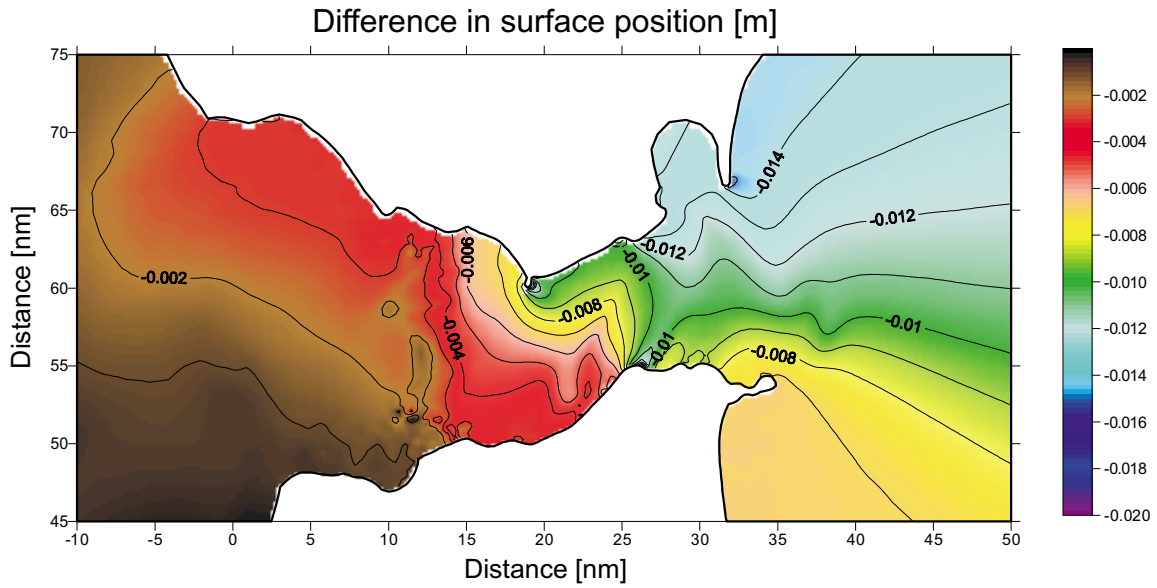

Fig. 4.8. Difference in the surface position between the two model runs assuming relative density differences between Atlantic and Mediterranean waters of 0.0021 and 0.0019 as well as a constant offset of the mean sea level at the Mediterranean boundary of –0.73 cm and +0.73 cm respectively (from Brandt et al. 2004a).

In the last years, especially due to the advent of satellite altimetry, large sea level changes in the Mediterranean have been observed (Cazenave et al. 2001). The recognition of the causes responsible for such changes is, however, complicated by the fact that the Mediterranean is not an isolated basin (Ross et al. 2000). Together with changes in the interior of the Mediterranean like, e.g., the warming trend in intermediate and deep water observed in the eastern basin since the early 1990s and in the western basin since the 1960s (Bethoux et al. 1990 1998; Cazenave et al. 2001), changes in the sea level of the Atlantic and in the exchange flow through the Strait of Gibraltar may be in fact important. Among the latter, changes of the hydraulic regime from submaximal to maximal and of the connected mixing strength have been proposed (Ross et al. 2000; Myers and Haines 2002). In the present work, we have focused our attention on the effect of changes in the density difference between Atlantic and Mediterranean waters on the sea level drop between the two basins. A trend in the sea level drop of O(1cm/yr) like, e.g., that observed between 1994 and 1997 (Ross et al. 2000) is explained by our model as the result of a trend in the relative density difference between the Mediterranean and Atlantic waters of O(10^{-4} 1/yr). Our numerical model allows also inferring, for the scenario of a changing density difference, the two-dimensional structure of the sea level variation. In Fig. 4.8 the difference in the mean sea surface elevation between the model runs carried out assuming relative density differences of 0.0021 and 0.0019 as well as a constant offset of the mean sea level at the Mediterranean boundary of –0.73 cm and +0.73 cm, respectively, is depicted. While, as expected, the sea surface elevation in the Atlantic approaches to the Strait of Gibraltar does not differ noticeably in the two experiments, the opposite is true in the Mediterranean approaches to the Strait of Gibraltar. There, both mean sea level elevations and its north-south gradient differ between the experiments. We note that the change in the sea level drop is larger at the northern shore than at the southern shore, which is in agreement with the observations reported by Ross et al. (2000). The reason for this behavior is the change in the exchange flow through the Strait of Gibraltar between both experiments. The stronger exchange flow in the run with a stronger density difference leads to a stronger along-strait velocity and, due to the effect of the Coriolis force, to a stronger north-south gradient in the surface elevation. Note, however, that a change in the exchange flow through the Strait of Gibraltar implies a change in the salt balance within the

Mediterranean and thus a change in the water mass salinity. A warming of the Mediterranean outflow, for instance, would lead to a decrease in the sea level drop between the two basins, but also to an increase of the salinity in the Mediterranean. The system would probably adjust to a new equilibrium, whose prediction would involve a realistic model of the whole Mediterranean.

5 Outlook

In this summary paper I have presented results of different process studies that are aimed at improving the physical understanding of ocean variability in key regions for ocean circulation and climate variability. The process studies presented here were based on a wide variety of methods. Among them are in-situ hydrographic and current observations from moored and shipboard instruments, or instruments lowered with the CTD rosette, remote sensing observations from the altimeters aboard the TOPEX/Poseidon and ERS satellites, the optical scanner aboard the SeaStar satellite, or the scatterometers aboard the ERS satellites as well as numerical simulations by different process oriented ocean models. Much effort has been put into the increase of measurement accuracy and/or range by applying new instruments, like e.g. the shipboard phased array Doppler current profiler (Fischer et al. 2003), new methods to analyze in-situ measurements, like e.g. application of an inverse method to lowered ADCP data by including shipboard ADCP data (Dengler et al. 2004), or new corrections to available datasets, like e.g. a correction of altimeter derived EKE with respect to the significant wave height (Brandt et al. 2004b). These efforts at the technical level are needed for gaining a better description of oceanic processes and their variability and, of course, for improving the physical understanding of these processes.

The overall goal of the oceanic process studies that I am involved in is an improved understanding of long-term changes in the ocean and the climate system. This can be achieved by allowing a better interpretation of long-term oceanic observations or by testing the realism of large and global scale ocean models. Exemplarily, I want to focus on two oceanic regions that are of particular interest in terms of climate variability and that are a major part of my current and planned research activities.

The first region is the Labrador Sea. This oceanic region is one of the focal points of Sonderforschungsbereich (SFB) 460 of the Leibniz-Institut für Meereswissenschften in Kiel. It is a region of great interest because of its role in water mass formation, thermohaline circulation, and possibly climate change. Moreover, it is one of the few sites of the World Ocean where open-ocean convection occurs, occasionally reaching great depths (Marshall and Schott 1999). In the present summary paper I have presented a study regarding the eddy field in the Labrador Sea as observed by satellite altimetry, which is a contribution to the subproject A8 of the SFB 460 (Brandt/Stramma). Among the main findings of this study are that although EKE is generated locally in the central Labrador Sea, the major part of the EKE propagates from the West Greenland Current (WGC) region into the central Labrador Sea. The WGC EKE that is generated by the instability of the WGC shows a strong interannual variability. However, the analysis of the altimeter data alone does not allow a quantification of the contribution of the eddy field to the preconditioning of the convection before the convective season or to the restratification after the convective season that is associated with transport of newly formed Labrador Sea Water (LSW) away from the convective region. Lilly et al. (2003) estimated from altimeter and in-situ data that eddies generated by the instability of the WGC are able to account for at most 25% of the necessary heat transport in the annual cycle. Katsman et al. (2004) suggested from high-resolution process modeling that, for a

realistic `end-of-winter'-state, these eddies are efficient in restratifying the convected water mass in the central Labrador Sea and are able to balance a significant portion of the atmospheric heat loss. Besides the seasonal changes of the stratification there are strong interannual changes: Hydrographic data from ship sections (Stramma et al. 2004) as well as from moored instruments in the central Labrador Sea revealed interannual changes in the Labrador Sea that are characterized by the increasing formation of lighter, upper LSW. The role of the eddy field for the interannual changes may be even more important than for seasonal changes. In fact, the interannual variability in the convection depth was not explainable in terms of the winter-to-winter variability of the local air-sea fluxes alone (Lazier et al. 2002). The strong interannual variability in the WGC EKE levels observed by altimetry may thus lead to year-to-year changes in the lateral fluxes transporting heat and salt from the WGC region into the central Labrador Sea, which must be accounted for in low-resolution climate models not resolving the eddy field in the Labrador Sea when realistic trends of convection depths should be simulated.

Using profiling float trajectories it was possible to track LSW along different pathways from the Labrador Sea toward the open North Atlantic (Fischer and Schott 2002). However, these observations are not able to resolve eddy processes in the central Labrador Sea. The analysis of altimeter data indicated higher EKE levels in the central Labrador Sea at the end of the convective season (Brandt et al 2004b). These observations together with boundary current measurements (Fischer et al. 2004) as well as high-resolution ocean modeling suggest that localized eddy processes and/or the instability of the Labrador Current system during winter could play an important role in the water mass exchange between central Labrador Sea, recirculation and Labrador Current. Within the subproject A8 of the SFB 460 we use acoustically tracked RAFOS floats to follow the pathways of the newly formed LSW. This project is a cooperation with a RAFOS project of A. Bower (WHOI) and S. Lozier (Duke) aimed at studying pathways of the LSW starting in the Labrador Current south of the convective region, which allows to use commonly acoustic sound sources deployed in the central Labrador Sea and the western subpolar North Atlantic. The positions of the RAFOS floats within our project can be determined three times per day instead of only once every ten days in the case of the profiling floats used before. The higher temporal resolution as well as the possibility to start the RAFOS mission during the convective season will give new inside in the water mass exchanges and the eddy processes in the central Labrador Sea.

The second region is the tropical Atlantic Ocean. In particular the eastern tropical Atlantic cold tongue is a region of great interest for a better understanding of climate variability. In particular, its interannual sea surface temperature (SST) variability is significantly correlated with land rainfall (Schott et al. 2004, “Tropical Atlantic Climate Experiment”, TACE, White Paper). In the present summary paper I have presented results regarding observations in the western tropical Atlantic along the 35°W section from 5°N toward the Brazilian coast. This section covers the eastward flowing undercurrents that are thought to be the main suppliers of the equatorial and eastern upwelling regions. Schott et al. (2002) found that in the undercurrent layer 80% of the northward flow at 5°S enters the Equatorial Undercurrent (EUC). In a recent model study, Hazeleger et al. (2003) calculated the model source regions of water transported eastward within the EUC and found that the overwhelming contribution to the EUC transport comes from subduction sites along the South Equatorial Current: one region in the southwest and one in the central subtropical South Atlantic. However, the model does not include realistic South and North Equatorial Undercurrents (SEUC, NEUC), possibly due the relative coarse model resolution. These currents are well represented in the shipboard observations along the 35°W section (Fig. 2.6) and seems to strengthen toward the central ocean. The transport carried within their shallower density layers is thought to supply partial inflow into the off-equatorial upwelling regimes along the coasts and in the Guinea

and Angola domes. Within a project financed by the German Science Foundation "Circulation of the shallow thermohaline subtropical-tropical cell of the Atlantic" (Schott/Brandt) the pathways within this cell will be studied using isopycnic RAFOS floats. The RAFOS floats that will be deployed during METEOR cruise M62/2 in August 2004 drift on different shallow density surfaces to follow the water masses in the tropical Atlantic Ocean. Isobaric APEX floats deployed during previous cruises appeared to move partly normal to isopycnal contours and are thus not able to follow the eastward flowing water masses that rise toward the sea surface.

An analysis of the seasonal mixed layer heat budget of the tropical Atlantic Ocean that was based on measurements from moored PIRATA buoys, near-surface drifting buoys, and a blended satellite in-situ SST product revealed the importance of the zonal temperature advection and the horizontal eddy temperature advection due to tropical instability waves in particular in the cold tongue region (Foltz et al. 2003). The authors concluded that for better estimates of the equatorial mixed layer heat balance in-situ estimates of subsurface velocity and temperature combined with horizontal gradients of velocity, temperature, and mixed layer depth are required. Results of our RAFOS project as well as results of current meter moorings at the equator at 35°W and at 23°W that are deployed in cooperation with the French EGEE program (B. Bourlès, LEGOS) will contribute to obtain better estimates of mean and eddy-induced advection. However, among the largest errors in the analysis of the SST variability in the cold tongue region is the highly unknown effect of vertical temperature entrainment. Thus, we proposed the purchase of a microstructure probe that could be used during our planned METEOR cruise in 2006 covering the western and central equatorial Atlantic Ocean. This cruise is aimed at understanding the zonal inflow toward the equatorial and eastern upwelling regions by measuring several meridional hydrographic and current sections crossing the equator between 35°W and 10°W. The use of the microstructure probe could additionally lead to better estimates of the vertical mixing in the near surface layer that provide a base from which interannual and decadal variability of the SST in the cold tongue region can be addressed.

In the future process studies will still be of great importance to identify and help to understand the role of different oceanic processes in the climate system of the earth. Observations will cover longer periods in time and the global scale in particular achieved by satellite remote sensing or self operating technologies, like e.g. ARGO floats and gliders. Additionally, high-precision in-situ observations from research vessels in limited oceanic regions or observations at key locations with moored instruments are needed to assess the realism and to identify drawbacks of ocean and climate forecast models.

6 Acknowledgements

I would like to thank my colleagues in Kiel Lothar Stramma, Jürgen Fischer, Marcus Dengler, Mario Müller, Uwe Papenburg, Carsten Eden, Andreas Funk, Rena Schoenefeldt, Karina Affler, Verena Hormann, Rainer Zantopp, Felix Morsdorf, Meike Hamann, Carlos Sena-Martins for instructive and stimulating conversation, for excellent teamwork during several research cruises and for cooperation in analyzing a large number of different data sets and model results. Special thanks go to Fritz Schott for continuous and generous support and valuable advice. Further I thank Angelo Rubino for his longstanding cooperation, Detlef Quadfasel, Burkard Baschek, Dmitri V. Sein for their involved participation in specific research studies.

7 References

Anderson, D. L. T., and P. B. Rowlands, The Somali Current responds to the Southwest Monsoon: the relative importance of local and remote forcing, *J. Mar. Res.*, **34**, 395-417, 1976.

Apel, J. R., L. A. Ostrovsky, and Yu. A. Stepanyants, Internal solitons in the ocean. Tech. Rep. MERCJRA0695, 70 pp., 1995 [Available from Milton S. Eisenhower Research Center, Applied Physics Laboratory, The Johns Hopkins University, Johns Hopkins Rd., Laurel, MD 20707.]

Armi, L and D. M. Farmer D.M., The flow of Mediterranean water through the Strait of Gibraltar, *Prog. Oceanogr.,* **21,** 1-105, 1988.

Baschek, B., U. Send, J. García Lafuente, J. Candela, Transport estimates in the Strait of Gibraltar with a tidal inverse model, *J. Geophys. Res.,* **106,** 31,033–31,044, 2001.

Beal, L. M., T. K. Chereskin, H. L. Bryden, and A. Ffield, Variability of water properties, heat and salt fluxes in the Arabian Sea, between the onset and wane of the 1995 southwest monsoon, *Deep-Sea Res. II,* **50 20**49-2075, 2003.

Bethoux, J. P., B. Gentili, J. Raunet, and D. Tailliez, Warming trend in the western Mediterrenean deep water, *Nature*, **347**, 660-662, 1990.

Bethoux, J. P., B. Gentili, and D. Tailliez, Warming and freshwater budget change in the Mediterranean since the 1940s, their possible relation to the greenhouse effect, *Geophys. Res. Letters*, **25**, 1023-1026, 1998.

Boebel, O., C. Schmid, and W. Zenk, Kinematic elements of Antarctic Intermediate Water in the western South Atlantic, *Deep-Sea Res. II* , **46**, 355-392, 1999.

Böning, C. W., and A. J. Semtner, High-resolution modeling of the thermohaline and wind-driven circulation, in *Ocean Circulation and Climate,* G. Siedler et al., Eds., Academic Press, 59–78, 2001.

Brandt, P., W. Alpers, and J.O. Backhaus, Study of the generation and propagation of internal waves in the Strait of Gibraltar using a numerical model and synthetic aperture radar images of the European ERS 1 satellite, *J. Geophys. Res.,* **101,** 14,237-14,252, 1996.

Brandt, P., A. Rubino, W. Alpers, and J. O. Backhaus, Internal waves in the Strait of Messina studied by a numerical model and synthetic aperture radar images from the ERS 1/2 satellites, *J. Phys. Oceanogr.,* **27,** 648-663, 1997.

Brandt, P., A. Rubino, D. Quadfasel, W. Alpers, J. Sellschopp, and H.-V. Fiekas, Evidence for the influence of Atlantic-Ionian Stream fluctuations on the tidally induced internal dynamics in the Strait of Messina, *J. Phys. Oceanogr.,* **29,** 1071-1080, 1999a.

Brandt, P., R. Romeiser, and A. Rubino, On the determination of characteristics of the interior ocean dynamics from radar signatures of oceanic internal solitary waves, *J. Geophys. Res.,* **104,** 30,039-30,046, 1999b.

Brandt, P., L. Stramma, F. Schott, J. Fischer, M. Dengler, and D. Quadfasel, Annual Rossby waves in the Arabian Sea from TOPEX/Poseidon altimeter and in-situ data, *Deep-Sea Res. II,* **49,** 1197-1210, 2002a.

Brandt, P., A. Rubino, and J. Fischer, Large-amplitude internal solitary waves in the North Equatorial Counter Current, *J. Phys. Oceanogr.*, **32,** 1567-1573, 2002b.

Brandt, P., M. Dengler, A. Rubino, D. Quadfasel, and F. Schott, Intraseasonal

variability in the southwestern Arabian Sea and its relation to the seasonal circulation, *Deep-Sea Res. II,* **50,** 2129 – 2141, 2003.

Brandt, P., A. Rubino, D. V. Sein, B. Baschek, A. Izquierdo, and J. O. Backhaus, Sea level variations in the western Mediterranean studied by a numerical tidal model of the Strait of Gibraltar, *J. Phys. Oceanogr.*, **34,** 433-443, 2004a.

Brandt, P., F. Schott, A. Funk, and C. S. Martins, Seasonal to interannual variability of the eddy field in the Labrador Sea from satellite altimetry, *J. Geophys. Res.*, **109**, C02028, doi:10.1029/2002JC001551, 2004b.

Brandt, P., and C. Eden, Annual cycle and interannual variability of the mid-depth tropical Atlantic Ocean, *Deep-Sea Res. II*, 2004, accepted.

Bruce, J. G., D. R. Johnson, and J. C. Kindle, Evidence for eddy formation in the eastern Arabian Sea during northeast monsoon. *J. Geophys. Res.*, **99**, 7651-7664, 1994.

Bryden, H. L. and T. H. Kinder, Recent progress in strait dynamics. *Rev. Geophys.*, **29**, 617-631, 1991.

Cane, M. A. and E. S. Sarachik, The response of a linear baroclinic equatorial ocean to periodic forcing, *J. Mar. Res.*, **39**, 651-693, 1981.

Cazenave, A., C. Cabanes, K. Dominh, and S. Mangiarotti, Recent sea level change in the Mediterranean sea revealed by TOPEX/Poseidon satellite altimetry. *Geophys. Res. Letters*, **28**, 1607-1610, 2001.

Cuny, J., P. B. Rhines, P. P. Niiler, and S. Bacon, Labrador Sea boundary currents and the fate of the Irminger Sea Water, *J. Phys. Oceanogr.*, **32**, 627-647, 2002.

Dengler, M., D. Quadfasel, F. Schott, and J. Fischer, Abyssal circulation in the Somali Basin, *Deep-Sea Res. II*, **49**, 1297-1322, 2002.

Dengler, M., F. A. Schott, C. Eden, P. Brandt, K. Affler, J. Fischer, and R. Zantopp, Deep Western Boundary Current eddies in the tropical South Atlantic, 2004, in preparation.

Eden, C., and C. Böning, Sources of eddy kinetic energy in the Labrador Sea, *J. Phys. Oceanogr.*, **32**, 3346-3363, 2002.

Evans, R. H., and O. B. Brown, Propagation of thermal fronts in the Somali Current System, *Deep-Sea Res.*, **28**, 521-527, 1981.

Farmer, D. M. and L. Armi, Maximal two-layer exchange over a sill and through the combination of a sill and contraction with barotropic flow. *J. Fluid Mech.*, **64**, 53-76, 1986.

Fischer, J., F. Schott, and L. Stramma, Currents and transport of the Great Whirl-Socotra Gyre system during the summer monsoon, August 1993, *J. Geophys. Res.*, **101**, 3573-3587, 1996.

Fischer, J., and F. Schott, Labrador Sea Water tracked by profiling floats - from the boundary current into the open North Atlantic, *J. Phys. Oceanogr.*, **32**, 573-584, 2002.

Fischer, J., P. Brandt, M. Dengler, M. Müller, and D. Symonds, Surveying the upper ocean with the Ocean Surveyor: a new phased array Doppler current profiler, *J. Atmos. Oceanic Technol.* 20**,** 742-751, 2003.

Fischer, J., F.A. Schott,and M. Dengler, Boundary circulation at the exit of the Labrador Sea, *J. Phys. Oceanogr.*, 2004, in press.

Foltz, G. R., S. A. Grodsky, J. A. Carton, and M. J. McPhaden, Seasonal mixed layer heat

budget of the tropical Atlantic Ocean, *J. Geophys. Res.*, 108, 3146, doi:10.1029/2002JC001584, 2003

França, C., I. Wainer, A. Mesquita, and G. Goni, Planetary equatorial trapped waves in the Atlantic Ocean from TOPEX/Poseidon altimetry, In: P. Malanotte-Rizzoli and G. J. Goni, eds., Interhemispheric Water Exchange in the Atlantic Ocean, Elsevier Oceanographic Series, **68**, 213-232, 2003.

Fratantoni, D.M., North Atlantic surface circulation during the 1990's observed with satellite tracked drifters, *J. Geophys. Res.*, **106**, 22,067-22,093, 2001.

Ganachaud, A., and C. Wunsch, Improved estimates of global ocean cir-culation, heat transport and mixing from hydrographic data, *Nature*, **408**, 453– 457, 2000.

Garrett, C., M. Bormans and K. Thompson, Is the exchange through the Strait of Gibraltar maximal or submaximal? In The Physical Oceanography of Sea Straits, edited by L. J. Pratt, pp. 271-294, Kluwer Academic Publishers, 1990.

Garternicht, U., Schott, F., Heat fluxes of the Indian Ocean from a global eddy-resolving model, *J. Geophys. Res.*, **102**, 21,147-21,159, 1997.

Greatbatch, R. J., and A. Goulding, Seasonal variations in a linear barotropic model of the North Atlantic driven by the Hellerman and Rosenstein wind stress field, *J. Phys. Oceanogr.*, **19**, 572-595, 1989.

Hazeleger, W., P. de Vries, and Y. Friocourt, Sources of the Equatorial Undercurrent in the Atlantic in a high-resolution ocean model, *J. Phys. Oceanogr.*, **33**, 677-693, 2003.

Helfrich, K.R., Time-dependent two-layer hydraulic exchange flows. *J. Phys. Oceanogr.*, **25**, 359-373, 1995.

Heywood, K. J., E. L. McDonagh, and M.A. White, Eddy kinetic energy of the North Atlantic subpolar gyre from satellite altimetry, *J. Geophys. Res.*, **99**, 22,525-22,539, 1994.

Izquierdo A., L. Tejedor, D.V. Sein, J.O. Backhaus, P. Brandt, A. Rubino, and B.A. Kagan, Control variability and internal bore evolution in the Strait of Gibraltar: A 2D two-layer model study, *Estuarine, Coastal and Shelf Science,* **53,** 637-651, 2001.

Karsten, R., H. Jones, and J. Marshall, The role of eddy transfer in setting the stratification and transport of a circumpolar current, *J. Phys. Oceanogr.,* **32,** 39–54, 2002.

Katsman, C. A., M. A. Spall, and R. S. Pickart, Boundary current eddies and their role in the restratification of the Labrador Sea, *J. Phys. Oceanogr.*, 2004, in press.

Kuznetsov, A. S., A. N. Paramonov, and Yu. A. Stepanyants, Investigation of solitary internal waves in the tropical zone of the western Atlantic. *Izv. Acad. Sci. USSR Atmos. Oceanic Phys.* 20, 840-846, 1984.

Labseagroup, The Labrador Sea Deep Convection Experiment, *Bull. Am. Meteorol. Soc.*, **79**, 2033-2058, 1998.

Latif, M. and T. P. Barnett, Interactions of the tropical oceans. *J. Climate*, **8**, 952-964, 1995.

Lavender, K.L., R.E. Davis, and W. Brechner Owens, Direct velocity measurements in the Labrador and Irminger seas describe pathways of Labrador Sea water, *Nature*, **407**, 66-69, 2000.

Lavender, K.L., R.E. Davis, and W. Brechner Owens, Observation of open-ocean deep convection in the Labrador Sea from subsurface floats, *J. Phys. Oceanogr.*, **32**, 511-526, 2002.

Lazier, J., The renewal of Labrador Sea Water, *Deep-Sea Res.*, **20**, 341-353, 1973.

Lazier, J., Temperature and salinity changes in the deep Labrador Sea, 1962-1986, *Deep-Sea Res.*, **35**, 1247-1253, 1988.

Lazier, J., R. Hendry, A. Clarke, I. Yashayaev and P. Rhines, Convection and restratification in the Labrador Sea, 1990-2000, *Deep-Sea Res.*, **49**, 1819-1835, 2002.

Lee, T., and Marotzke, J., Inferring meridional mass and heat transports of the Indian Ocean by fitting a general circulation model to climatological data. *J. Geophys. Res.*, **102**, 10585-10602, 1997.

Leetmaa, A., D. R. Quadfasel, and D. Wilson, Development of the flow field during the onset of the Somali Current 1979, *J. Phys. Oceanogr.*, **12**, 1325-1342, 1982.

Lilly, J. M., P.B. Rhines, F. Schott, K. Lavender, J. Lazier, U. Send, and E. D'Asaro, Observations of the Labrador Sea eddy field, *Prog. Oceanogr.*, **59**, 75-176, 2003.

Lux, M., H. Mercier, and M. Arhan, Interhemispheric exchanges of mass and heat in the Atlantic Ocean in January – March 1993, *Deep-Sea Res. I*, **48**, 605– 638, 2001.

MacKinnon, J. A., and M. C. Gregg, Shear and Baroclinic Energy Flux on the Summer New England Shelf. J. Phys. Oceanogr., **33**, 1462-1475, 2003.

Marshall, J. and F. Schott, Open-ocean convection: observations, theory and models, *Rev. Geophys.*, **37**, 1-64, 1999.

Marshall, J. H. Jones, R. Karsten, and R. Wardle, Can eddies set ocean stratification? *J. Phys. Oceanogr.,* **32,** 26–38, 2002.

Myers, P. G., and K. Haines, Stability of the Mediterranean's thermohaline circulation under modified surface evaporative fluxes. *J. Geophys. Re*s., **107**, art. no. 3021, 2002.

McCreary, J. P., Equatorial beams, *J. Mar. Res.*, **42**, 395-430, 1984.

McCreary, J. P., P. K. Kundu, and R. L. Molinari, A numerical investigation of dynamics, thermodynamics and mixed-layer processes in the Indian Ocean. *Prog. Oceanog.*, **31**, 181-244, 1993.

Moum, J.N., D.M. Farmer, W.D. Smyth, L. Armi and S. Vagle, Structure and generation of turbulence at interfaces strained by internal solitary waves propagating shoreward over the continental shelf. *J. Phys. Oceanogr*., **33** 2093-2112, 2003.

Munk, W., and C. Wunsch, Abyssal recipes II: energetics of tidal and wind mixing. *Deep-Sea Res.*, **45** 1977-2010, 1998.

Ostrovsky, L. A., and Yu. A. Stepanyants, Do internal solitons exist in the ocean? *Rev. Geophys.*, **27**, 293-310, 1989.

Philander, S. G. H., Forced oceanic waves, *Reviews of Geophysics and Space Physics*, **16**, 15-46, 1978.

Pickart, R. S., D. J. Torres, and R. A. Clarke, Hydrography of the Labrador Sea during active convection, *J. Phys. Oceanogr.*, **32**, 428-457, 2002.

Pinkel, R., Internal solitary waves in the Warm Pool of the Western Equatorial Pacific, *J. Phys. Oceanogr.,* **30,** 2906-2926, 2000.

Prater, M., Eddies in the Labrador Sea as Observed by Profiling RAFOS Floats and Remote Sensing, *J. Phys. Oceanogr.*, **32**, 411- 427, 2002.

Qiu, B., W. Miao, and P. Müller, Propagation and decay of forced and free baroclinic

Rossby waves in off-equatorial oceans, *J. Phys. Oceanogr.*, **27**, 2405-2417, 1997.

Radko, T., and J. Marshall, Eddy-Induced Diapycnal Fluxes and Their Role in the Maintenance of the Thermocline, *J. Phys. Oceanogr.*, **34**, 372-382, 2004.

Reverdin, G., P. P. Niiler, H. Valdimarsson, North Atlantic surface currents, *J. Geophys. Res.*, **108**, 3002, doi:10.1029/2001JC001020, 2003.

Ross, T., C. Garrett, and P.-Y. Le Traon, Western Mediterranean sea-level rise: changing exchange flow through the Strait of Gibraltar, *Geophys. Res. Letters*, **27**, 2949-2952, 2000.

Rubino A., P. Brandt, and R. Weigle, On the dynamics of internal waves in a nonlinear, weakly nonhydrostatic three-layer ocean, *J. Geophys. Res.,* **106,** 26,899-26,916, 2001.

Schott, F., Monsoon response of the Somali Current and associated upwelling, *Prog. Oceanogr.*, **12**, 357-381, 1983.

Schott, F., J. Fischer, U. Garternicht, and D. Quadfasel, Summer monsoon response of the northern Somali Current 1995, *Geophys. Res. Letters*, **24**, 2565-2568, 1997.

Schott, F., and J. Fischer, Winter monsoon circulation of the northern Arabian Sea and Somali Current, *J. Geophys. Res.*, **105,** 6359-6376, 2000.

Schott, F., and J. P. McCreary, The monsoon circulation of the Indian Ocean, *Prog. Oceanogr.*, **51,** 1-123, 2001.

Schott, F. A., P. Brandt, M. Hamann, J. Fischer, and L. Stramma, On the boundary flow off Brazil at 5-10°S and its connection to the interior tropical Atlantic, *Geophys. Res. Letters,* **29(17),** 1840, doi:10.1029/2002GL014786, 2002.

Schott, F., M. Dengler, R. Schoenefeldt, The shallow overturning circulation of the Indian Ocean, *Prog. Oceanogr.*, **53**, 57-103, 2002.

Schott, F. A., M. Dengler, P. Brandt, K. Affler, J. Fischer, B. Bourles, Y. Gouriou, R. L. Molinari, and M. Rhein, The zonal currents and transports at 35°W in the tropical Atlantic, *Geophys. Res. Letters*, **30(7),** 1349, doi:10.1029/2002GL016849, 2003.

Sengupta, D., R. Senan, and B. N. Goswami, Origin of intraseasonal variability of circulation in the tropical central Indian Ocean, *Geophys. Res. Letters*, **28**, 1267-1270, 2001.

Shankar, D., and S. R. Sheyte, On the dynamics of the Lakshadweep high and low in the southeastern Arabian Sea, *J.Geophys. Res.*, **102**, 12551-12562, 1997.

Spall, M. A., and R. S. Pickart, Wind-driven recirculations and exchanges in the Labrador and Irminger seas, *J. Phys. Oceanogr.*, **33**, 1829-1845, 2003.

Stammer, D., and C. Wunsch, Temporal changes of eddy energy of the oceans, *Deep-Sea Res. II,* **46,** 77-108, 1999.

Stammer, D., C. Böning, and C. Dieterich, The role of variable wind forcing in generating eddy energy in the North Atlantic, *Prog. Oceanogr.,* **48,** 289-311, 2001.

Stammer, D., K. Ueyoshi, and C. Wunsch, Geographic variations and temporal changes in the ocean eddy transports, submitted to *J. Phys. Oceanogr.*, 2004.

Stramma, L., P. Brandt, F. Schott, D. Quadfasel, and J. Fischer, Winter and summer monsoon water mass and heat transport changes in the Arabian sea near 8°N, *Deep-Sea Res. II,* **49,** 1173-1195, 2002.

Stramma, L., M. Rhein, P. Brandt, M. Dengler, C. Böning, and M. Walter,

Warmwatersphere circulation in the western tropical Atlantic in boreal fall 2000, *Deep-Sea Res. II*, 2004a, submitted.

Stramma, L., and D. Kieke, M. Rhein, F. Schott, I. Yashayaev, K. P. Koltermann, Deep water changes at the western boundary of the subpolar North Atlantic during 1996 to 2001, *Deep-Sea Res.*, 2004b, submitted.

Subrahmanyam, B., I. S. Robinson, J. R. Blundell, and P. G. Challenor, Indian Ocean Rossby waves observed in TOPEX/Poseidon altimeter data and in model simulations, *Int. J. Remote Sensing*, **22**, 141-167, 2001.

Swallow, J.C. and J.G. Bruce, Current measurements off the Somali coast during the Southwest Monsoon of 1964, *Deep-Sea Res.*, **13**, 861-888, 1966.

Swallow, J. C. and M. Fieux, Historical evidence for two gyres in the Somali Current, *J. Mar. Res.*, **40** (Suppl.), 747-755, 1982.

Swallow, J. C., R. L. Molinari, J. G. Bruce, O. B. Brown, and R. H. Evans, Development of near-surface flow pattern and water mass distribution in the Somali Basin in response to the Southwest Monsoon of 1979, *J. Phys. Oceanogr.*, **13**, 1398-1415, 1983.

Thierry, V., A. M. Treguier, and H. Mercier, Numerical study of the annual and semi-annual fluctuations in the deep equatorial Atlantic Ocean, *Ocean Modelling*, **6**, 1-30, 2003.

Vauclair, F. and Y. du Penhoat, Interannual variability of the upper layer of the tropical Atlantic Ocean from in situ data between 1979 and 1999, *Climate Dyn.*, **17**, 527-546, 2001.

Vlasenko, V., P. Brandt, and A. Rubino, Structure of large-amplitude internal solitary waves, *J. Phys. Oceanogr.,* **30,** 2172-2185, 2000.

Weisberg, R. H. and T. Y. Tang, A linear analysis of equatorial Atlantic Ocean thermocline variability, *J. Phys. Oceanogr.*, **20**, 1813-1825, 1990.

Willebrand, J., S. G. H. Philander, and R. C. Pacanowski, The oceanic response to large-scale atmospheric disturbances, *J. Phys. Oceanogr.*, **10**, 411-429, 1980.

Wirth, A., J. Willebrand, and F. Schott, Variability of the Great Whirl from observations and models, *Deep-Sea Res. II*, **49**, 1279-1295, 2002.

Wunsch, C., Global problems and global observations, in *Ocean Circulation and Climate,* G. Siedler et al., Eds., Academic Press, 47–58, 2001.

Zebiak, S. E., Air-sea interaction in the equatorial Atlantic region, *J. Climate*, **6**, 1567-1586, 1993.